
Article:
Adams, C., Conte, M. orcid.org/0000-0002-1399-0344, Alborzi, E. orcid.org/0000-0002-2585-0824 et al. (3 more authors) (2024) Exploring homolytic aromatic substitution as a driver for fuel deposition with quantum chemistry and experiments. Fuel, 360. 130470. ISSN 0016-2361

https://doi.org/10.1016/j.fuel.2023.130470

EXPLORING HOMOLYTIC AROMATIC SUBSTITUTION AS A DRIVER FOR FUEL DEPOSITION WITH QUANTUM CHEMISTRY AND EXPERIMENTS

Charlie Adams,[*,†] Marco Conte,[‡] Ehsan Alborzi,[*,†] Anthony JHM Meijer,[†] Kevin Hughes,[†] and Mohamed Pourkashanian [*,†]

†*Department of Mechanical Engineering, The University of Sheffield, Sheffield, S3 7RD, UK* ‡*Department of Chemistry, The University of Sheffield, Sheffield, S3 7RD, UK*

E-mail: cadams2@sheffield.ac.uk; e.alborzi@sheffield.ac.uk; mohamed.pourkashanian@sheffield.ac.uk

Abstract

Liquid phase insoluble formation in fuels can cause performance and safety issues. To understand the formation of insolubles in fuels from first principles, a series of density functional theory (DFT) calculations were run to calculate the energetic barriers of the autoxidation and coupling reactions for several common fuel aromatics/heteroatoms. The six compounds chosen were phenol, toluene, naphthalene, pyrrole, quinoline, and indole. Using a combination of DFT calculations and gravimetric and petroxy experimental work, a novel homolytic aromatic substitution (HAS) coupling pathway was identified for each compound. While previous studies have treated deposition steps implicitly, our detailed calculations of HAS reactions and bulk fuel (RH) oxidation reaction barriers afforded the

development of bespoke pseudo-detailed mechanisms for each aromatic compound with explicit reaction steps. These mechanisms were then used to predict trends in deposition behavior of the compounds tested in a simple *n*-dodecane surrogate. The novel HAS mechanism suggested for fuels was proposed to start with the reaction of an aromatic radical (Ar·) to an aromatic (ArH), which then formed a radical (ArHAr·) σ-intermediate. It was then found that hydroperoxides (ROOH) could re-aromatize the radical intermediate (ArHA·), forming a deposit dimer (ArAr). Although our sensitivity analysis revealed that alkyl fuel radical and fuek alkoxyl radical abstraction steps influenced the final mass of the deposit, the Ar.+ArH HAS coupling step was found to have the largest influence. Finally, an aromatic/heteratom model containing phenol and toluene was built, which showed that phenol suppressed deposition from toluene, and peaked in deposit mass at a phenol:toluene ratio of 25:75. Although our study was limited to Ar self-reactions, we hypothesize that bulk fuel – aromatic coupling could also be governed by HAS reactions, allowing researchers to move towards a more first-principles based deposition model..

Keywords: Density Functional Theory, Homolytic Aromatic Substitution, Thermal Stability, Jet Fuel, Pseudo-detailed Mechanism

1. Introduction

The formation of insolubles in the liquid-phase of jet fuels is mainly driven by the formation of oligomers from fuel components.[1, 2] Oligomers successively grow starting from dimers, trimers, tetramers and so on. Each oligomer growth step is predominantly characterized by the formation of C–C and C–O bonds. Previous research has emphasized the termination of antioxidant and/or fuel aromatic components (Ar· + Ar· → Ar_2) as a key source of fuel

insolubles, and by that extension C–C/C–O bond formation.[3, 4, 5] This has led Heneghan and Zabarnick to highlight an inverse correlation between the ease of oxidation and the formation of deposits. In other words, a fuel with a lower oxidation rate arises from the higher concentration of chain-breaking Ar· radicals, and therefore have a higher concentration of Ar· to undergo termination steps producing deposit.[3] However, in some instances, this relation does not always hold. Notably, some nitrogen compounds like pyrroles and indoles tend to show low/no effects on autoxidation rates yet are severe deposit promoters.[6, 7, 8] To explain these exceptions, Heneghan and Zabarnick propose that some fuels produce termination Ar–Ar products with a higher solubility.[3] Nevertheless, there may be other chemical factors that need to be explored.

The formation of Ar–Ar via the termination of two free-radicals Ar· in solution is part of an oxidative coupling process. However, it is possible to form Ar–Ar without a termination step under oxidative conditions. Focusing on transition metal free processes, homolytic aromatic substition (HAS) has received considerable attention as a method for cross-coupling aromatic compounds under free-radical conditions.[9, 10, 11, 12] Additionally, HAS mechanisms have been used as a way to understand the rate of radical reactions.[13, 14] The general mechanism of HAS is shown in Figure 1.1. First, an attack of an aryl radical to an arene compound generates a σ-intermediate. The σ-intermediate is then re-aromatized via elimination of a leaving group forming a dimer. In this sense, HAS reactions are analogous to electrophilic aromatic substitution (EAS) reactions, except that the σ-intermediate is not charged. EAS reactions have been proposed as a mechanism in the formation of jet fuel deposits.[15] However, in aprotic non-polar jet fuel, the stabilization of charged EAS σ-intermediates is precluded.[16] By contrast, HAS reactions have been shown to readily occur in non-polar aprotic solvents between arenes under molecular oxygen.[17] In general HAS reactions have presented a challenge to organic chemists due to poor selectivity, leading to

intractable mixtures.[11] Nevertheless, in the context of jet fuel fouling, fuel deposits and gums are characterized by highly disordered coupled products composed of mainly aromatic groups.[18, 19] Overall, the HAS reactions between aromatic fuel species should be investigated as possible route to deposits. Particularly as HAS offers a route to form C–C bonds without terminating the free-radical chain mechanism, and can instead be considered a propagation step.

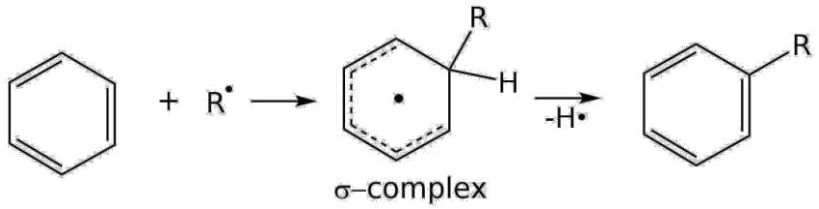

Figure 1.1: Generalized HAS mechanism, where an Ar· radical attacks a generic aromatic species. This attack subsequently forms a sigma-complex, which is in a doublet state. The sigma complex is re-aromatized by the loss of a hydrogen *via* an unspecified mechanism.

Several reactions for the formation of insolubles/deposits are represented in pseudo-detailed mechanisms in the public literature.[5, 20] However, at present, they are implicit. As a result, they do not represent specific chemical transformations, but are composed of 'pseudo' species with parameters fitted to experiments. In the future, a wider range of fuel chemistries and blends will require predictive mechanisms with greater sensitivity to the starting components, without relying too heavily on fitting parameters. However, due to complexity and range of insoluble structures, a compromise needs to be met between the range of reactions and products represented.

92 In recent years, density functional theory (DFT) has become a popular tool to build pseudo-
93 detailed mechanisms jet fuel deposition from 'first-principles'.[21, 22] DFT allows direct
94 calculations of thermochemical and kinetic data, and evaluation of competing chemical
95 reaction pathways. By contrast, previous pseudo-detailed mechanisms have been produced
96 by producing activation energies from fitted experimental data.[5, 20] However, this leads
97 to mechanisms which are only suitable for specific types of fuel.

98 It is the aim of this paper to: 1) explore the possibility of HAS as a route to insolubles
99 formation and 2) attempt to predict insoluble formation tendencies using DFT methods. First,
100 several two-component fuels containing bulk and heteroatoms will be stressed to produce an
101 insoluble mass. Then, the energetic pathways from fuel heteroatoms and bulk species to
102 dimers are calculated and compared to insolubles generated by the surrogate fuels. As a
103 means of understanding the deposition process further, the solubility of oligomers will be
104 considered too.

105 2 Methods and Materials

106 2.1 Surrogate Fuels for this Study

107 Six surrogate fuels were built with a range of compounds designed to represent the different
108 heteroatom and aromatic compounds found in fuels. Out of the nitrogen class of compounds
109 pyrrole (Sigma Aldrich, >98% purity), quinoline (Oakwood chemicals, >98% purity), and
110 indole (Sigma Aldrich, >99% purity) were selected.

111 Pyrrole and indole are two 5-membered nitrogen heteratom compounds known to promote
112 insoluble formation, with pyrrole being a particularly problematic insoluble promoter.[8, 23]
113 Quinoline has been shown to also promote insolubles, but to a lesser degree than pyrrole and

114 indole.[8, 7] Next, phenol (ACROS Organics, >99%) was chosen to represent the phenolic
115 class of compounds, again shown to promote insolubles in a variety of real and surrogate
116 fuels.[8, 24, 25, 26] Finally, two aromatic components, naphthalene (Fluorochem, >99%)
117 and toluene (SLS, 99.5%) were chosen for their presence in the mono-aromatic and di-
118 aromatic class in fuels.[27] Each of the above six components were added as 0.1 mol l^{-1} to
119 *n*-dodecane (ACROS Organics, >99%).

120 The authors acknowledge that the chosen concentration of 0.1 mol l^{-1}, equivalent to
121 approximately 20,000 ppm of aromatics, is significantly higher than the heteroatom levels
122 typically found in real fuels, which generally range from 100 to 1000 ppm.[51] However,
123 even at this high concentration, the amount of deposit generated from 5 ml of surrogate fuel
124 was relatively low. Therefore, the fuel needed to be spiked with this level of deposit for the
125 study given the sensitivity of the gravimetric deposit measurement equipment. Furthermore,
126 the primary focus of this study was to investigate the coupling between aromatics in the
127 presence of hydrogen abstraction and addition reactions, hence the requirement for a high
128 concentration of aromatic species to ensure dominant Ar-Ar reactions. Nevertheless, in a
129 real fuel scenario, fuel-aromatic reactions would likely be more prevalent. While homolytic
130 aromatic substitutions would still be relevant (including for fuel-Ar reactions), their impact
131 on the coupling reactions between different species would be more challenging to validate
132 due to the increased complexity of coupling pathways.[14]

133 Another aspect of the design of the surrogate fuels in this study which differ from real fuels
134 was the selection of unsubstituted aromatics. Real fuel aromatics have multiple alkyl-
135 substitutions round the ring aromatic ring. We chose to investigate unsubstituted compounds
136 as a ‘base-case’ for the coupling reactions here. This base-case was chosen here so that gross
137 differences in aromatic classes could be explored. Future studies adding substituted groups

would add another dimension to the work, where the effect of substitutions *within and between* each compound class could be explored. Moving beyond the base-case towards a more realistic fuel molecule, additional alkyl- substitutions would likely have two effects based on EAS and HAS theory: 1) block reactive sites where alkyl- substitutions are present and 2) act as weak directing groups.[11] There is also the possibility that alkyl-substitutions would affect the solubility, which can be explored in future work via the methods detailed in section 2.2.

2.2 Method of Thermal Stressing and Deposit Measurement

To produce the insoluble masses, 5 ml of fuel was added to a 50 ml borosilicate round bottom pressurized flask. The flask was heated to 140°C for 24 h under 1 bar constant oxygen supply. The flask was sealed to all gases aside from the supplied oxygen. After heating, the flask was allowed to cool and insolubles were then filtered through a 0.1 µm glass fibre filter to give the total weight of insolubles in the bulk. The flask was then washed with trisolvent and then washed into a flask. The flask was then dried in a vacuum oven to remove any liquid residue, weighed, and then compared with the weight of the clean flask- giving the total weight of adherent insolubles left in the flask.[28] The sum of the insolubles weights on the filter and in the flask gave a mass total insolubles per surrogate. The deposit experiments were repeated at least 3 times for each surrogate to improve the accuracy of the total insolubles measurement.

A petroOxy device was used to produce oxygen depletion curves for each surrogate fuel. The petroOxy device is a sealed gold-lined chamber in which 5 ml of fuel is thermally

159 stressed at 140°C. The headspace above the heated fuel is depleted as the fuel is stressed,
160 giving a measure of the rate of oxygen consumption in the bulk fuel.

161 2.3 Hansen Solubility Parameters and Computational Details

162 All calculations were performed in Gaussian09 (E.01) using the B3LYP
163 functional.[29][30] Grimme's DFT-D3(BJ) dispersion correction was applied to all the
164 calculations to account for long-range effects.[31] A PCM solvation model, with n-
165 dodecane as the chosen solvent, was selected to replicate the hydrocarbon bulk.[32] The
166 basis set chosen was cc-pVTZ on an ultrafine grid. This basis set adds polarization
167 functions, allowing orbital hybridization to be taken into account.[33] Transition states
168 were optimized using the QST1/3 method depending on the reaction studied. All transitions
169 states were verified by the presence of one imaginary frequency corresponding to the
170 saddle point. Additionally, intrinsic reaction coordinate (IRC) calculations were performed
171 to verify the transition state corresponded to the expected reactants and products.
172 Unrestricted (broken symmetry) calculations were performed on open-shell systems, where
173 the HOMO and LUMO were mixed (guess=mix option). Entropy values were corrected
174 using the GoodVibes script, which employs a quasi-harmonic correction corrected at
175 298K.[34, 35, 36]

176 In Hansen solubility theory, three Hansen solubility parameters (HSPs) are assigned to
177 each molecule: D for dispersion, P for polarity, and H for hydrogen bonding. As a
178 consequence, each solvent exists in a 3-dimensional space of HSPs. The HSP distance
179 between two molecules in the 3d HSP space is given by:

$$Ra^2 = 4(D_1 - D_2)^2 + (P_1 - P_2)^2 + (H_1 - H_2)^2 \quad (1.1)$$

Where R_a is the Hansen distance.

The HSP parameters for the test solvents were either obtained from the HSPIP dataset or calculated using the software. The HSPIP software requires a series of test solvents/solutes, tested for their solubility in the *n*-dodecane. A score 0 is assigned to insoluble solvents and a score of 1 is assigned to soluble solvents.

In each case, 0.1 mol l^{-1} of each test compound was added to 5ml of *n*-dodecane. Resulting from the series of tests is a 'sphere' in 3d HSP space, whose dimensions are determined by the solubility of the sphere (Figures 2.1 and 2.2). The radius of sphere R_0 is then used to asses the solubility of a proposed solvent, where R_a of the test molecule is used in the following equation:

$$RED = R_a/R_0. \quad (10.2)$$

Where RED stands for Relative Energy Difference. A RED > 1 implies the molecule is likely insoluble in your main solvent (*n*-dodecane in this case), whereas a RED < 1 implies the molecule is soluble. Our calculated sphere was composed of 13 lab grade compounds known for their presence in fuel and gave a fit of 1 according to HSPIP software. The results for these tests are presented in Table 2.1 . Here it is important to acknowledge that the solubility of the deposit precursors in pure *n*-dodecane this study will likely be different to a conventional fuel due to the presence of aromatic compounds and minor components. Nevertheless, these parameters are useful to understand insoluble formation our surrogate fuel, and to improve the HSP method for future studies.

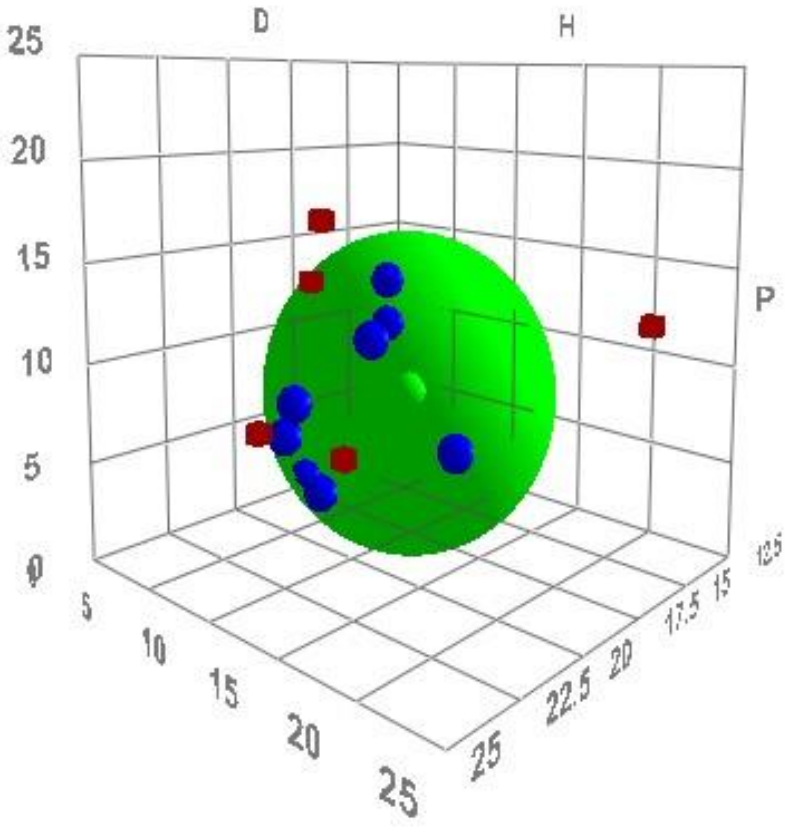

202

203 Figure 2.1: HSPIP Sphere

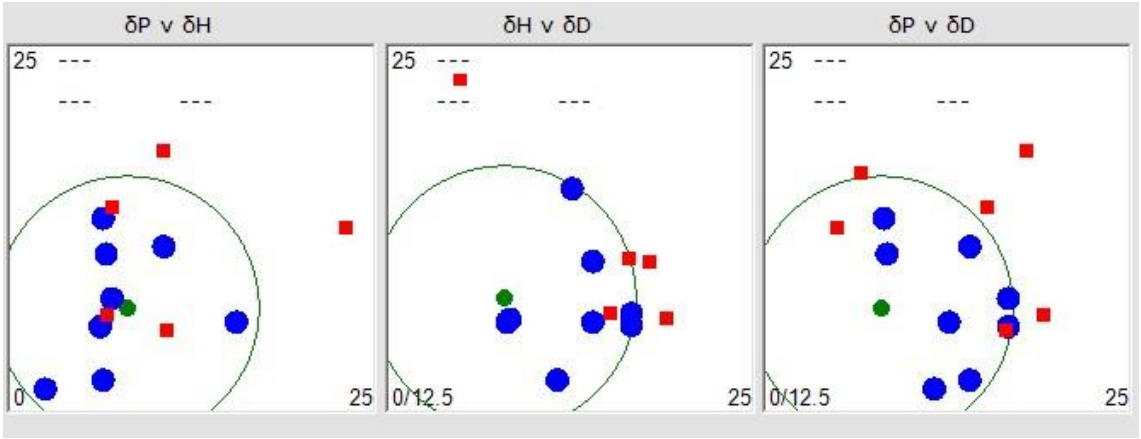

204

205 Figure 2.2: HSPIP Sphere parameter fits

206

207

Table 2.1: Hansen Solubility test solvents and their Associated HSPs. The sphere gave a fit of 1.000

Solvent	Database/Calculated HSP	D	P	H	Score	RED
Indigo	Calculated	21.10	17.4	10.0	0	1.639
Carbazole	Database	21.7	6.4	6.2	0	1.243
p-Benzoquinone	Database	19.8	13.7	6.5	0	1.121
Water	Database	15.5	16.0	42.3	0	4.042
2-Naphthol	Database	20.4	5.4	10.2	0	1.000
Methanol	Database	14.7	12.3	22.3	0	1.800
Di-*n*-Butyl Sulfoxide	Database	16.4	10.5	6.1	1	0.443
Naphthalene	Database	19.2	2.0	5.9	1	0.884
Pyrrole	Database	19.2	11.0	10.0	1	0.863
Dipropyl Sulfone	Database	16.3	12.9	5.9	1	0.705
Toluene	Database	18.0	1.4	2.0	1	0.961
Indole	Database	20.5	7.5	6.5	1	0.973
Phenol	Database	18.5	5.9	14.9	1	0.979
Quinoline	Database	20.5	5.6	5.7	1	0.995

2.4 Pseudo-Detailed Mechanism in Fuels

In order to compare the total insolubles to the number of dimers predicted by DFT, several new reaction steps were proposed which will be elucidated in the results and discussion. To

capture the autoxidation reactions in the bulk, the basic autoxidation scheme (BAS) was used which gave good agreement with oxygen and hydroperoxide depletion with experiment. The BAS scheme was optimized for a range of C10-C14 hydrocarbons, whereby the thermochemical and kinetic parameters were obtained using *n*-dodecane as the model fuel. Further details of the BAS scheme can be found in reference.[22] To construct the mechanism, the Eyring equation was used, with A being formed from the calculated entropy barrier and E_a formed from the calculated enthalpy barrier. All the forward and reverse barriers were calculated from a stable pre-reaction and post-reaction complex.

For each surrogate fuel, different mechanisms were constructed to study oxygen depletion and deposit formation. For oxygen depletion, the level of oxygen was fixed at 1.8 mmol l^{-1}.[37] For the deposition mechanism, oxygen was removed as a limiting reagent (kept constant at 1.8 mmol l^{-1}) to reflect the continuous supply of oxygen in our deposit forming rig. The mechanism was integrated in MATLAB using the **ode45** solver. The mechanism gave a molar concentration of a dimer, which was then related to a mass via the molecular weight of the proposed dimer.

3 Results and Discussion

3.1 Homolytic Aromatic Substitution Mechanism

The key bottleneck in any HAS reaction is the re-aromatization and liberation of hydrogen from the σ-intermediate. The loss of H· in this step is not well understood. Nevertheless, one paper exploring HAS reactions between aryl iodides and arenes using oxygen as an oxidant, proposed a re-aromatization step involving oxygen this is shown as reaction 1) in Figure 3.1 Because hydroperoxides (ROOH) and oxygenated species like alcohols (ROH) form under

oxidative conditions in fuels, these were also considered as possible reagents to remove hydrogen from the σ-intermediate. ROOH reacting with the σ-intermediate is proposed to form RO· and H_2O, is shown as reaction 2) in Figure 3.1. ROH reacting with the σ-intermediate is proposed to form R· and H_2O, is shown as reaction 3) in Figure 3.1.

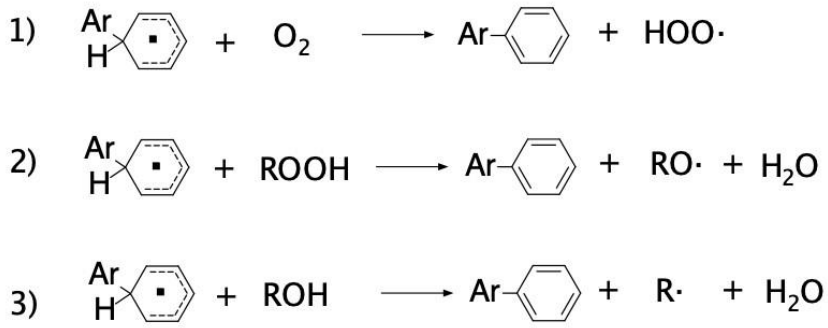

Figure 3.1: HAS reactions considered for fuel coupling reactions. Each step shows the σ-intermediate formed from an Ar· + ArH reaction, and the species chosen to re-aromatize the intermediate.

Considering the mechanisms presented in Figure 3.1, we explored the possibility of these reactions in phenolic coupling. Phenols have widely been recognized as being detrimental to fuel thermal stability.[8] HAS mechanisms have previously been considered as a possible pathway the oxidative coupling of phenols.[14] Nevertheless, it should be noted that in a real fuel, direct phenol-phenol coupling is not likely to be dominant to the concentration of phenolic compounds. However, the main of this section is to understand the possible re-aromatization step available to fuel species. The findings here will be used as a template for other fuel HAS reactions.

The calculated HAS pathways for phenol are presented in Figure 3.2. First, the formation of the σ-intermediate is endergonic and has a free-energy barrier of $^{\ddagger}G$=+25.64kcalmol ^{1} leading to an intermediate PhOPhO·. The para- position of the phenol was chosen as the site

of oxidative coupling of another phenoxy radical given that this is the generally the more favorable site.[38] The first mechanism in Figure 3.1, involving the re-aromatization with oxygen, could not be identified for phenol. A key challenge with the oxygen transition state is the choice of spin multiplicity. Given that oxygen is in the triplet state, and the system σ-intermediate is in the doublet state, an open-shell doublet or a quartet surface can be chosen.

The other two mechanisms presented in Figure 3.1 involve ROH and ROOH. The ROOH pathway in Figure 3.2 shows a lower barrier to re-aromatization of the intermediate compared to the ROH by 30.22 kcal mol^{-1}. Additionally, the ROOH is thermodynamically favored, namely due to the enhanced stability of the RO· radical compared to R· The IRCs for both these pathways are presented in Figures S.1 and S.2 in the SI. The ROOH and ROH re-aromatization transition states are characterized by a rotation of the terminal OH moiety towards an available hydrogen at the para-coupling site.

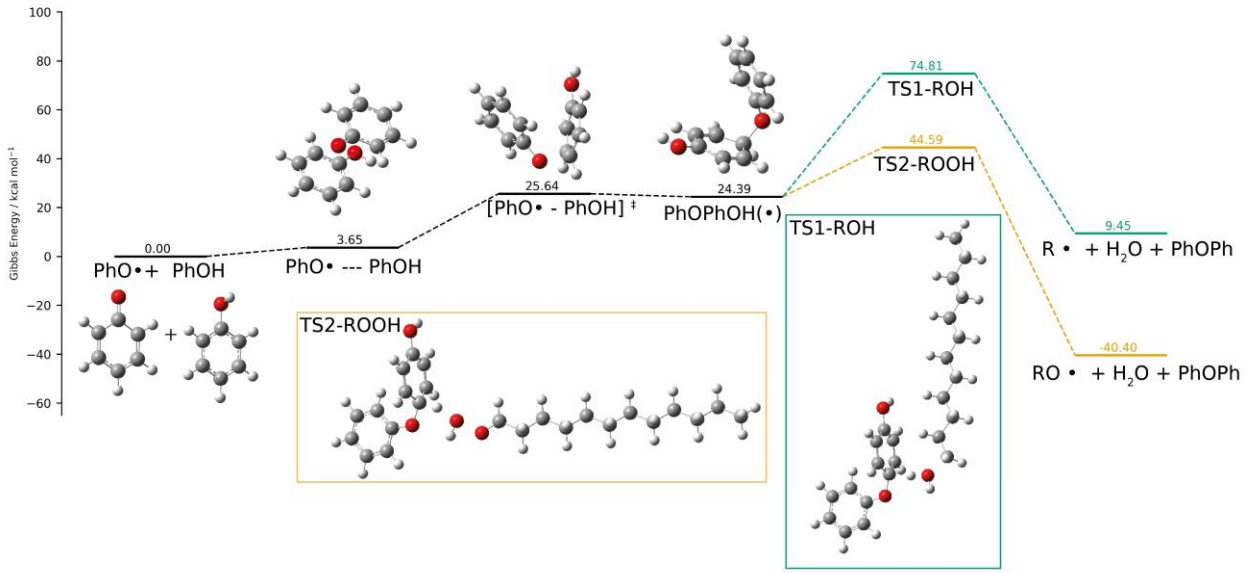

Figure 3.2: Comparison of different HAS pathways at the B3LYP-D3//cc-pVTZ level of theory using *n*-dodecane (PCM) as a solvent. The first step of the process in black shows the Ar· + ArH---ArHAr· reaction of a phenol and a phenoxy radical, leading to the σ-

intermediate. The subsequent levels in green shows the re-aromatization step with ROH and the level in orange shows the re-aromatization step with an ROOH species.

3.2 Comparison of Antioxidant Oligomer Solubility and Pathway to Deposit

To justify the assumption that the formation of insolubles results from the coupling of ArH species, we calculated Hansen solubility parameters for oligomers for our chosen heterotoms of increasing size. Previous research has hypothesized that aromatic compounds in fuel rapidly become insoluble as they grow in size.[43] Figure 3.3 shows the change in RED score as the oligomer chain grows, where relative energy difference (RED) > 1 indicates an oligomer that has become insoluble in *n*-dodecane. For real fuels, these results will vary, particularly as the aromatic content will increase the 'likeness' of the solvent to other extended aromatic structures.[39] Nevertheless, because our model fuels in this study contain *n*-dodecane as the base solvent, the Hansen plots here are a useful tool to explore deposition tendency in our model fuels. Oligomer structures were chosen based on the favored coupling site for each heteratom based on literature data and our calculations.[38, 40, 41, 42] The phenol chain growth is shown as an example. What is clear is that in general as the oligomer grows, the solubility in *n*-dodecane decreases. However, different oligomers reach the insolubility threshold in fewer units, where a single unit is the monomer, 2 units is a dimer and so on. For example, comparing toluene and naphthalene, naphthalene reaches the insolubility threshold after 2 units have coupled. This is consistent with previous observations that di-aromatics form deposit more rapidly because they 'require fewer consecutive reaction steps to produce high-molecular-weight'.[43]

Interestingly, heteroatom size does not influence the solubility of the resultant oligomers. Instead, the lower solubility is related to the dD parameter in the HAS framework, representing Van Der Waals forces between the solvent and heteroatom. As the oligomers grow, the difference in polarity and hydrogen bonding begins to decrease (indicated by the decreasing dP and dH parameters), but the difference in dispersion forces dD increases.

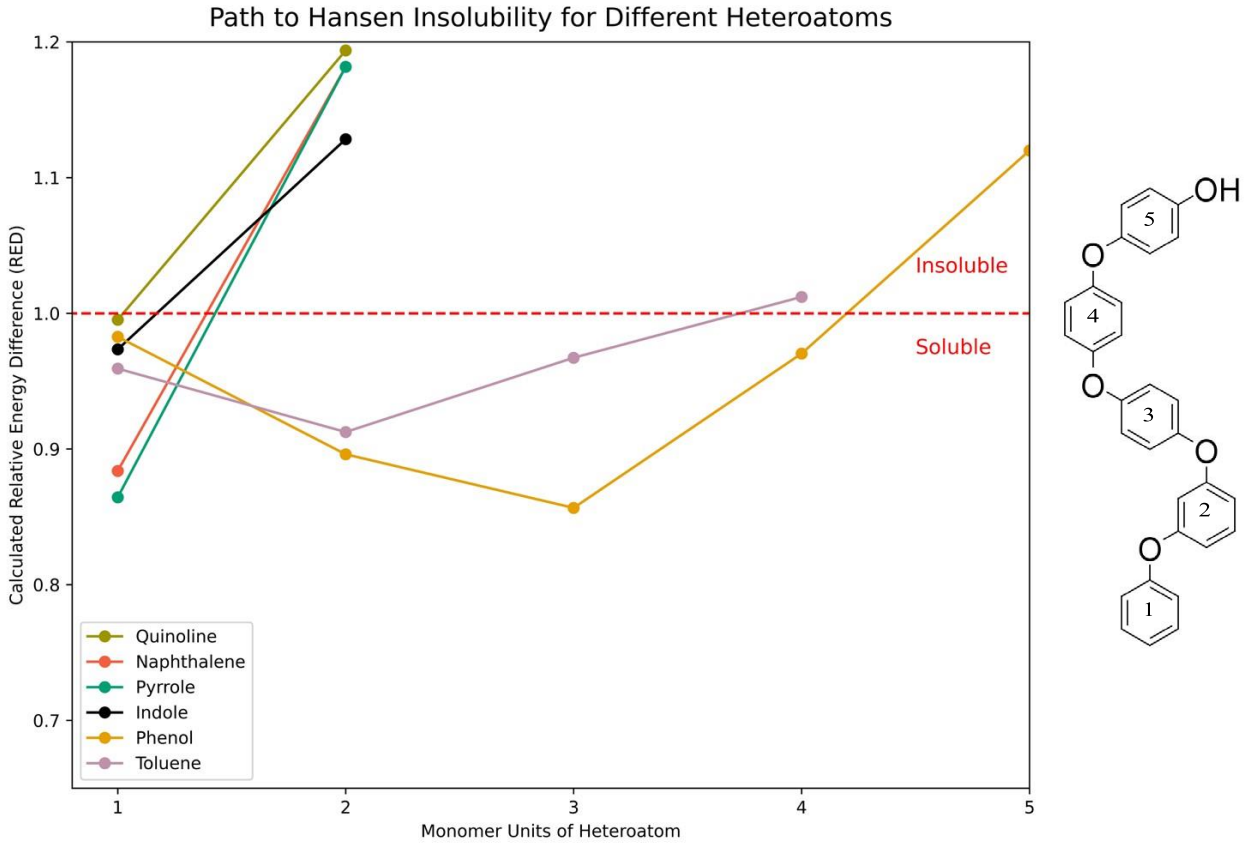

Figure 3.3: Effect of oligomer unit size on solubility calculated using the HSPiP software. It is clear some heteroatoms reach insoluble threshold in fewer units than others. Phenol and toluene is particularly interesting, becoming initially more soluble in *n*-dodecane before reaching the threshold. For phenol this is due to the growth of oligomer leading to a lower proportion of the molecule containing the *H*-bonding –OH group, but as the molecule grows the Van Der Waals dD difference grows eventually leading to an insoluble.

3.3 Predicting Deposition formation using DFT

3.3.1 H-abstraction and Coupling Mechanisms for Each Heteratom

Based on the solubility modelling presented in Figure 3.3, it was clear that the coupling of fuel heteratoms would lead to insoluble formation in our *n*-dodecane surrogate. Following the proposed HAS pathway, we calculated the H-abstraction and subsequent barriers to form dimers via the HAS pathway. The barriers for these reactions are presented in detail in Table S.1 of the appendix. The termination reaction was barrierless for all the species, and the pre-exponential factor was kept constant for each of the species at 3×10^9.[5]

The H-abstraction site and the coupling site for each species was selected based on literature and our own testing, and is summarized in Figure 3.4. For phenol, H-abstraction occurs at the O-site, with coupling between the subsequent phenoxy radical and the para-carbon site of a phenol.[38] For naphthalene, the C3 site was favored over the C2 position in terms of both abstraction and coupling barrier heights. For quinoline, the C2 site is the most favored site for coupling and H-abstraction, and the barriers for abstraction were lower at the C2 site compared to the C3 site.[44] For toluene, the para position was selected for coupling and H-abstraction based on our own testing and literature data.[45]

For indole and pyrrole, the favored coupling and H-abstraction site were found to be different. For indole, the N1 site was found to be the most favorable site for H-abstraction, but the C3 site is the most favored for coupling. Nevertheless, C–N linkages are detected very rarely and are found to be thermodynamically prohibited for indole oligomers.[46, 47] As a consequence, we compared the overall pathway to dimers at the C3 position via H-abstraction at the N1 and C3 positions. The results for the indole dimer formation calculations are found in Figure S.4 of the SI. Overall, the C3 H-abstraction pathway shows

the highest barriers. Therefore, the N1 H-abstraction pathway for indole was chosen. Similarly, for pyrrole, H-abstraction at the N1 position is favored, yet polypyrrole is formed of C2-C2 linkages.[40] Comparing both pyrrole coupling C2 coupling pathways with H-abstraction at the N1 or C2 position, presented in Figure S.3, both pathways have similar barrier heights. Nevertheless, the initial H-abstraction reaction at the N1 position is more favorable and leads to an intermediate I1b *G* 24.49 kcal mol^{-1} lower in energy that the C2 pathway. As a consequence, following the N1 pathway, pyrrole would have antiox-

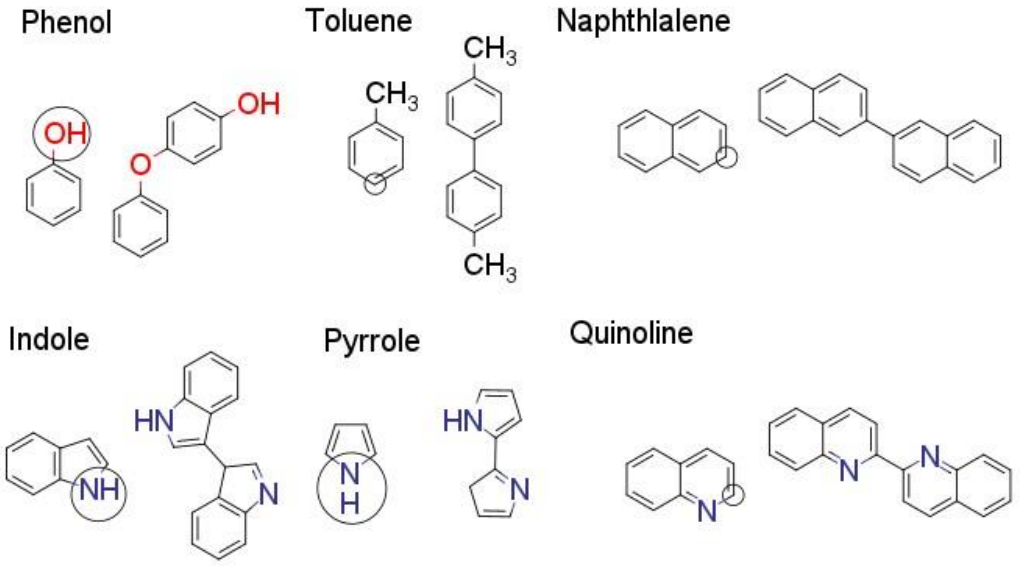

Figure 3.4: H-abstraction Sites and Dimers Selected for the Pseudo-Detailed Mechanisms. The selected H-abstraction site is circled, and resultant dimer is shown for each species.

idant properties, which is reflected in the petroOxy measurements (Figure 3.6b). Therefore, the N1 abstraction pathway for pyrrole was chosen.

Regarding the different coupling and H-abstraction sites for indoles and pyrroles, it should be underlined that this difference may only be relevant to self-reactions. Indeed, for indole

345 and pyrrole functionalization reactions under oxidative conditions, the N- group is pre-
346 protected prior to arylation and alkylation reactions. [52,40]

347 Based on the above proposed coupling and H-abstraction sites, we computed the barriers for
348 ArH species reacting with *n*-dodecane R·,RO·, and ROO· radicals and subsequently forming
349 dimers via a HAS process. The Gibbs potential energy surfaces for our chosen heteroatoms
350 undergoing H-abstraction to the formation of dimers are presented in Figure 3.3 for RO·.
351 The values for the reactions with the other radicals are presented in Table S.1 of the SI.

352 The first section (reaction A) of Figure 3.5, showing the abstraction of hydrogen from our
353 selected ArH species. Here, we can see there is a clear difference in the reactivity and
354 thermochemistry. To begin with, phenol shows the lowest barriers for hydrogen abstraction
355 out of all the species tested. Phenol has long been known as a powerful antioxidant in
356 fuels.[5] By contrast, toluene exhibits the highest barrier and the overall Gibbs energy
357 abstraction reaction is endergonic at +28.32kcalmol ^{1}. The overall order of the Gibbs energy
358 barrier to hydrogen abstraction (section A) is, in descending order: toluene > naphthalene >
359 quinoline > pyrrole > indole > phenol.

360 The resultant radicals formed indicate that phenol, pyrrole, and indole all exhibit
361 antioxidant properties, by undergoing an exergonic H-abstraction reactions. By contrast,
362 naphthalene, toluene, and quinoline undergo endergonic H-abstraction reactions showing
363 no antioxidant qualities. At this point in the reaction process, two Ar· radicals can terminate
364 to form a dimer. Nevertheless, this termination process is a rare occurrence due to the low-
365 concentration of Ar· species in fuel (for example, for pyrrole the peak concentration in our
366 mechanism was 5.17E-13 mol l^{-1}).

The HAS reaction between an Ar· and ArH first proceeds with an attack of the radical. The radical attack is shown as pathway B) in Figure 3.5. For this step, the antioxidant species formation is endergonic and proceeds with high Gibbs energy barriers for phenol and indole of $‡G$ 25.63 kcal mol^{-1} and $‡G$=24.36 kcal mol^{-1} respectively. By contrast, pyrrole proceeds with a lower barrier of $‡G$=19.20 kcal mol^{-1}. On the other hand, the non-antioxidant species show lower barriers for pathway B). In fact, naphthalene and toluene show the highest barriers for the H-abstraction step, but lowest barriers out of all the species for step B) at $‡G$=12.87 kcal mol^{-1} and $‡G$=13.50 kcal mol^{-1} respectively. Additionally, the formation of the intermediate is the most exergonic for naphthalene and toluene. The relationship between the antioxidant tendency and the ease of coupling is likely related to the aromatic structure. Species with more antioxidant qualities will also have higher levels of aromaticity to stabilize radicals, but also will have higher barriers to aromaticity-breaking radical attack.

The final step in the dimer forming process is the re-aromatization step *via* loss of hydrogen from the intermediate. Interestingly, the barriers for this step are similar for our aromatics tested, in the range of 23.87-17.47 kcal mol^{-1}. This step is clearly less related to the structure of the ArH compound. Nevertheless, the concentration of ROOH available to complete this step, is related to the antioxidant qualities of the ArH species in fuels. For example, for phenols, due to their antioxidant properties, the concentration of ROOH is expected to be low.[24] As a consequence, termination reactions likely provide a higher source of C–C/C–O coupling. To explore how these interrelated pathways yield deposits for different fuel components, we created different pseudo-detailed mechanisms to compare each fuel.

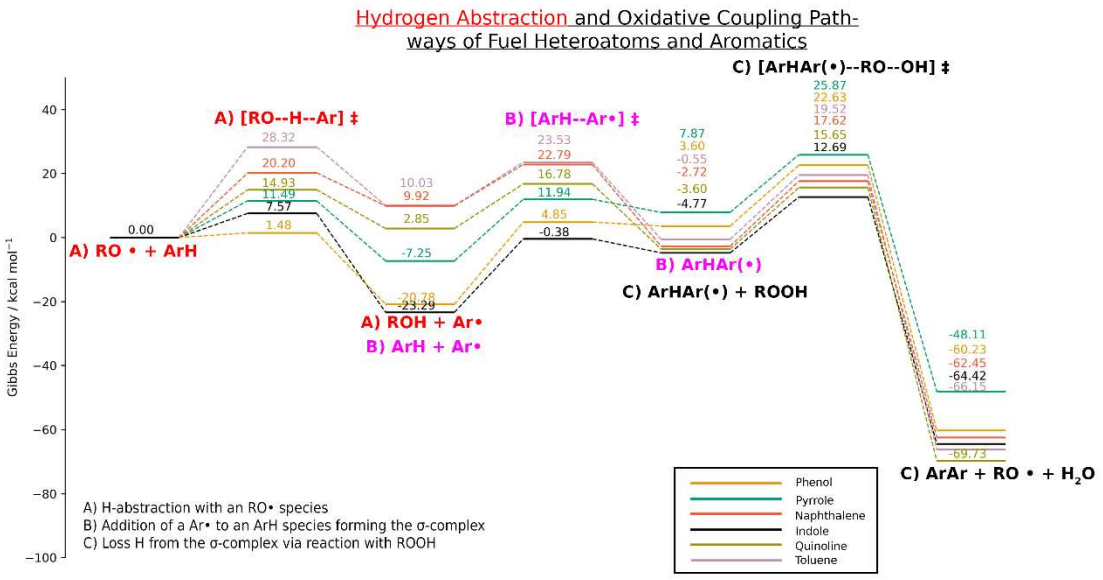

390

391 Figure 3.5: Growth to a deposit dimer for our chosen heteroatoms, calculated at the B3LYP-
392 D3/cc-pVTZ *n*-dodecane PCM level of theory. The barriers were calculated from stable pre-
393 reaction complexes. The R species was *n*-dodecane. The antioxidant species (phenol, indole
394 and pyrrole) show exergonic H-abstraction in step Ar.

395

396

397

398 3.3.2 Comparison of Experimental Results and Psuedo-Detailed Models

399 **Antioxidant Behavior**

400 First, the antioxidant behavior of our surrogate fuels was explored in relation to our models.
401 The O_2 depletion predicted by our model alongside the petroOxy depletion curves are
402 presented in Figure 3.6. Although the petroOxy device cannot measure the O_2 depletion in
403 the bulk, the device can be used to assess the antioxidant behavior of different fuels.[76] Our

404 model successfully predicts that pyrrole, indole, and phenol are all antioxidant species, as
405 shown by the increased induction period in thepetroOxy curves. In addition, the petroOxy
406 device indicates that indole and phenols are stronger antioxidants than pyrrole, which is also
407 reflected in the O_2 depletion curves in our mechanism. However, the difference between
408 indole and phenol in the petroOxy curves is not reflected in the mechanism.

409 **Deposition Behavior**

410 The amount of insoluble dimers predicted by our model compared with the total insolubles
411 measured is presented in Figure 3.7. It should be noted that the comparison here is focused
412 on the *correlation* between amount of dimers predicted and total deposit produced by
413 experiment. As a consequence, the correlation produced will reflect how well the model
414 predicts deposition behavior. Indeed, the difference between correlated and measured
415 deposits by a factor of ~300. This is due to the fact our mechanism only focuses on the
416 formation of dimers. Dimers are likely only to form a small proportion of the total deposit
417 structure, hence the large different in mass. Instead, the results here intend to explore how
418 well the model predicts couple propensity between different species which we hypothesize
419 is related to the ease of forming dimers. The model predicts the insoluble formation behavior
420 between our different surrogates well, with pyrrole producing the largest amounts of
421 insolubles. Interestingly, phenol and indole are shown to produce the lowest amount of
422 deposit in both our experiments and model. By contrast, in real fuels, indoles, and
423 particularly phenol concentration are shown to correlate well with final insoluble mass.[8]
424 A key difference between our simplified surrogates and real fuels are the synergistic effects
425 between fuel classes, which are not captured in our two-component surrogates. In particular,
426 sulfur is shown to interact strongly with 5-membered nitrogen heterocycles, and phenols
427 with other nitrogen compounds.[7, 48] For example, in a simplified surrogate, previous work

has shown trends between deposition propensity of 5- and 6-membered heterocycles break down, where quinoline-like compounds have shown to produce more deposit than indole compounds.[7] Nevertheless, the use of surrogates is still important to understand the chemical interactions within species classes.

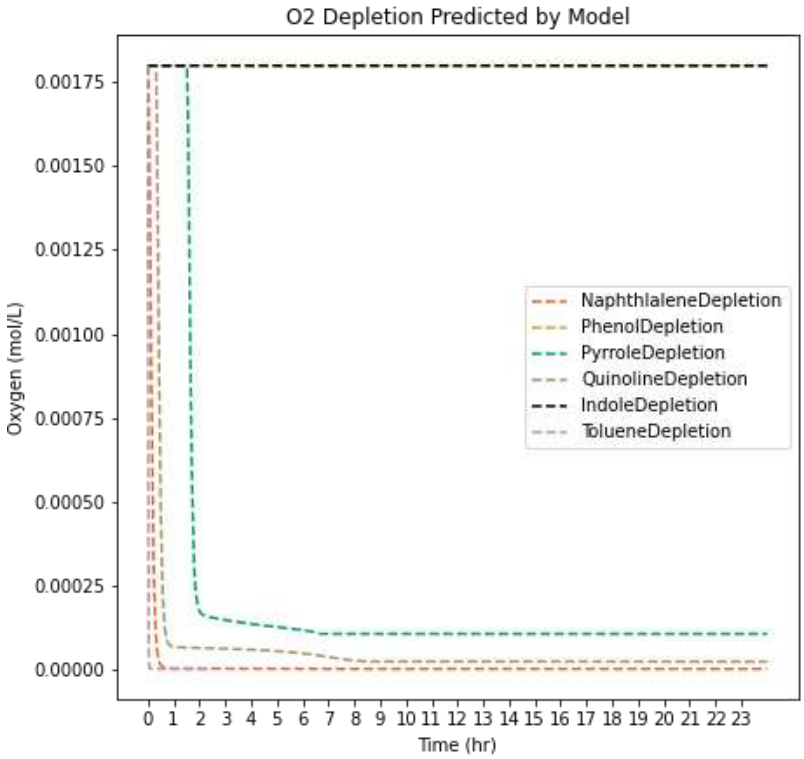

(a) O_2 Depletion Predicted by our model

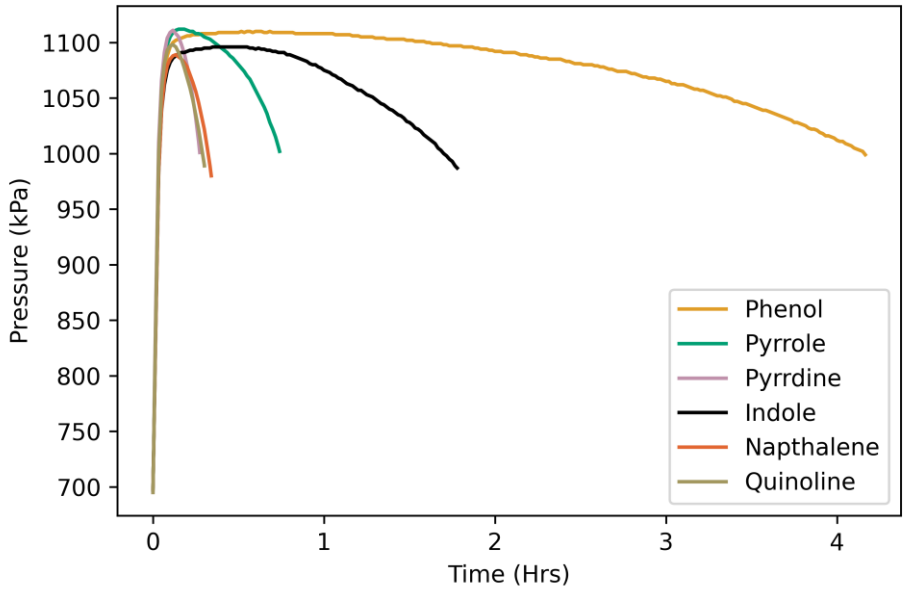

(b) Petroxy depletion behavior

Figure 3.6: O_2 depletion behavior of our surrogate- comparison between model and experiment. The model shows the change in O_2 concentration over time. The petroOxy depletion curves show the change in headspace pressure, and although they are not a direct measure of O_2 depletion, they can differentiate between antioxidant qualities of different species.

Interestingly, in our experiment and models, toluene and naphthalene produced more insolubles than phenol and indole. This is interesting as fuel thermal degradation is often viewed as solely driven by heteroatoms.[25] Exploring the barriers for toluene and naphthalene in detail in Table S.1, we see that lower barriers to the ArH + Ar·→ ArHAr· reaction are found with the aromatic species. Sensitivity analysis (Figure 3.9) of our models suggests this coupling step is strongly related to the final insoluble mass. However, in a 2-component fuel, combining an antioxidant heteroatom and aromatic, the formation of aromatic insolubles will be significantly reduced due to the size of the H-abstraction barrier in comparison to the other heteroatoms used in this study (Figure 3.5). Instead, the

heteroatom antioxidant class will form the majority of the Ar· radicals going on to form deposit. To strengthen this hypothesis, using our calculated values, a fuel model was built containing both phenol and toluene.

The effect of heteroatoms suppressing deposition from non-antioxidant species is demonstrated in Figure 3.8, where insolubles are generated from pseudo-detail model fuels containing different ratios of toluene and phenol is tested. The model was built using the same BAS scheme base described in the section 2.4, with the addition of both toluene and phenol pathways. In this simplified model, toluene-derived insolubles are suppressed upon introduction of phenol. This effect can help explain why fuel deposits/insolubles often have an elemental composition of heteroatoms higher than conventional fuels also containing aromatic hydrocarbons.[49] Another interesting effect of blending is the peak in phenol insolubles at 25:75 phenol:toluene ratios above a 100% phenol mix, which implies that above a certain concentration, phenols will prevent the formation of insolubles. The peak concentration of hydroperoxide steadily drops at different % phenol concentrations, which is related to the extent the autoxidation chain is suppressed. The peak of phenol deposition could be related to the ROOH concentration, allowing more σ-intermediates to be re-aromatized. This shows our model can replicate the effect of changing concentrations of antioxidant on total insolubles.

For some of the fuels the pseudo-detailed mechanisms reflect the behavior of 'peak' deposition temperature. The effect of temperature on the concentration of deposits for each mechanism is shown in Figures S.6-10 of the SI. For quinoline, a peak deposition level is reached at 460K. Whereas for toluene, as the temperature increases the level of deposit decreases. All the other fuel models show an increase in concentration of deposit as the temperature rises. This demonstrates these deposit mechanisms can reflect the complex

474 behavior of observed in real fuels of increasing and decreasing levels of deposit depending
475 on fuel temperature.[50]

476 Finally, our results here lend credence to a HAS pathway leading to deposit. When the HAS
477 pathway is removed from the mechanism in Figure 3.7b, no discernable trend is found
478 between the formation of dimers and insolubles measured. In fact, the HAS pathway appears
479 particularly important for species with low/no antioxidant tendency, but with a tendency to
480 still form insolubles.

481 Sensitivity analysis of our bespoke mechanisms in presented in Figure 3.9. The reaction
482 numbers cited here correspond to those given in Table S.1. For our mechanisms, the reaction
483 29, Ar· + ArH → ArHAr·, has the largest influence on the level of deposit with the exception
484 of phenol. Increasing the rate of reaction 29 leads to more ArHAr· species which can readily
485 form deposit. Reaction 32, Ar· + ROOH → ArH + ROO·, removing hydroperoxides from
486 the system also has an influence on the level of deposit. As the rate of reaction 32 increases,
487 hydroperoxides are removed from the system leading to fewer ArHAr· + ROOH re-
488 aromatization reactions leading to deposit dimers. The change of ROOH and insoluble
489 concentration presented in Figure 3.10 demonstrates that as insolubles are produced ROOH
490 is depleted. For all the species tested, the RO· (reaction 26) and R· (reaction 27) hydrogen
491 abstraction steps have a large influence on the level of deposit, with faster rates leading to
492 more Ar· species able to undergo coupling reactions. By contrast, the rate of the ROO·
493 abstraction barrier (reaction 16) has a negligible influence on deposition for most species
494 because this reaction in general has high barriers already. Finally, for phenol, reaction 26,
495 ArH + R→ Ar· + RH also influences the formation of deposit more than the other species,
496 and is more important than the coupling step (reaction 29). This is likely because the

497 termination pathway dominates the formation of deposits here, thus leading to a direct
498 correlation between the concentration of Ar· and the amount of deposit dimer.

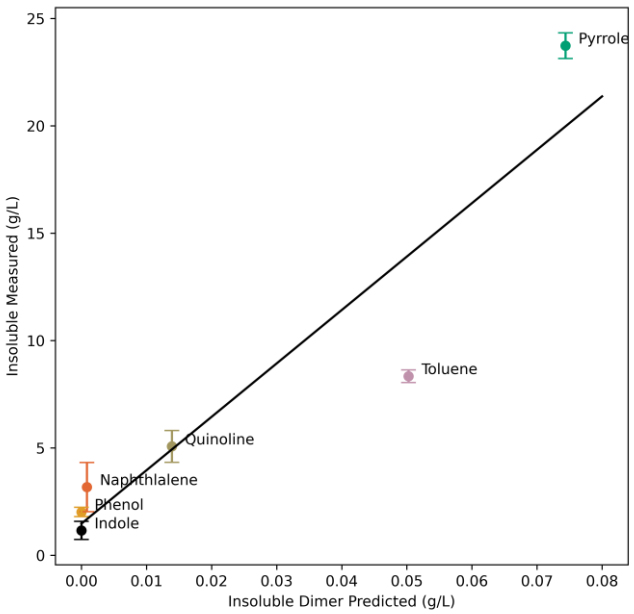

(a) Correlation between mass of dimer predicted by our model and insolubles measured.

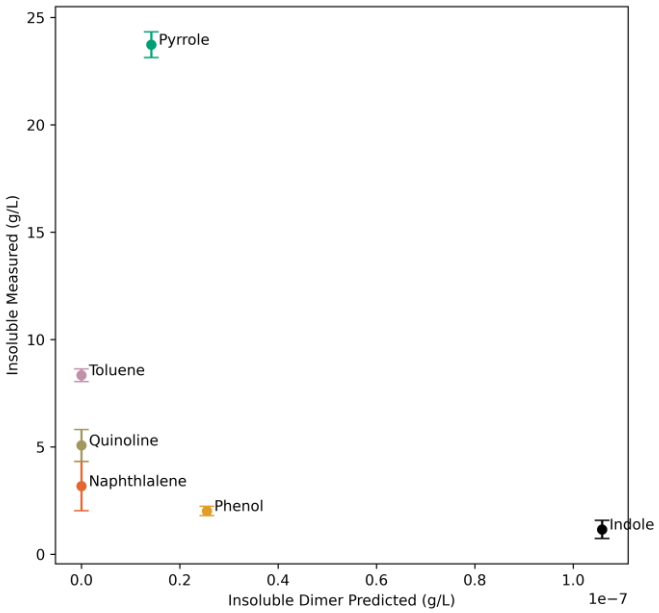

(b) Correlation between mass of dimer predicted by our model and insolubles measuredwhen the HAS pathway is excluded.

Figure 3.7: Insoluble formation behavior- comparisons between model and experiment. Temperature of the experiment and psuedo-detailed *n*-dodecane chemical mechanism containing the A and E_a values shown in Table S.1. The temperature was set at 431 K both the model and the experiment.

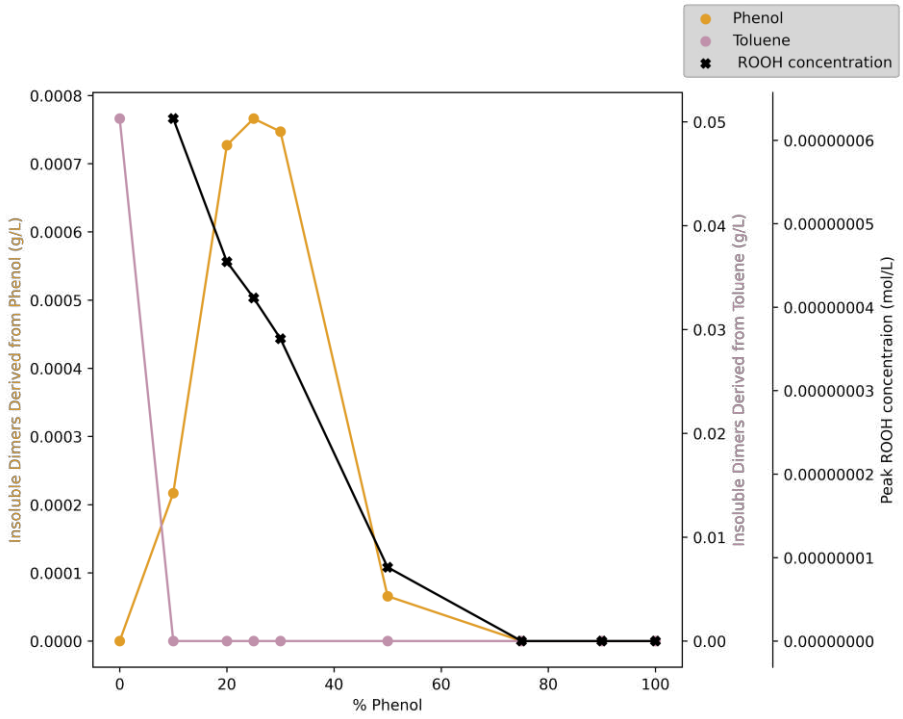

Figure 3.8: Effect of phenol % in a phenol toluene aromatic total of 0.1 mol L^{-1} on the insolubles derived from phenol and toluene.

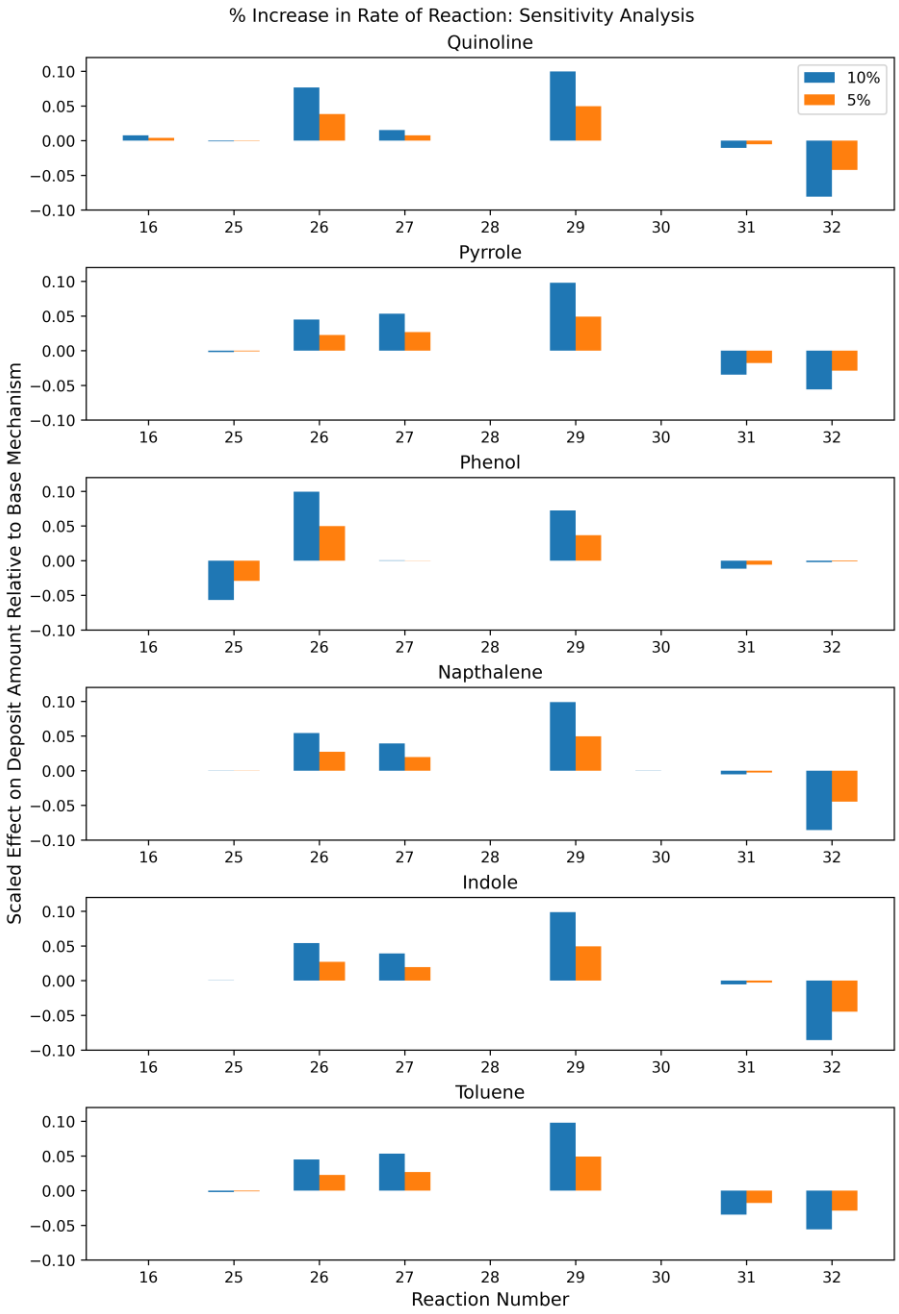

511

512 Figure 3.9: Sensitivity analysis of the bespoke insoluble pseudo-detailed mechanisms. For
513 the sensitivity analysis, the rate of reaction is increased by a factor of 10% (blue) and 5%
514 (orange) and the resultant increase in insolubles is shown relative to the base pseudo-
515 detailed mechanism. The reaction number corresponds to Table S.1 in the SI

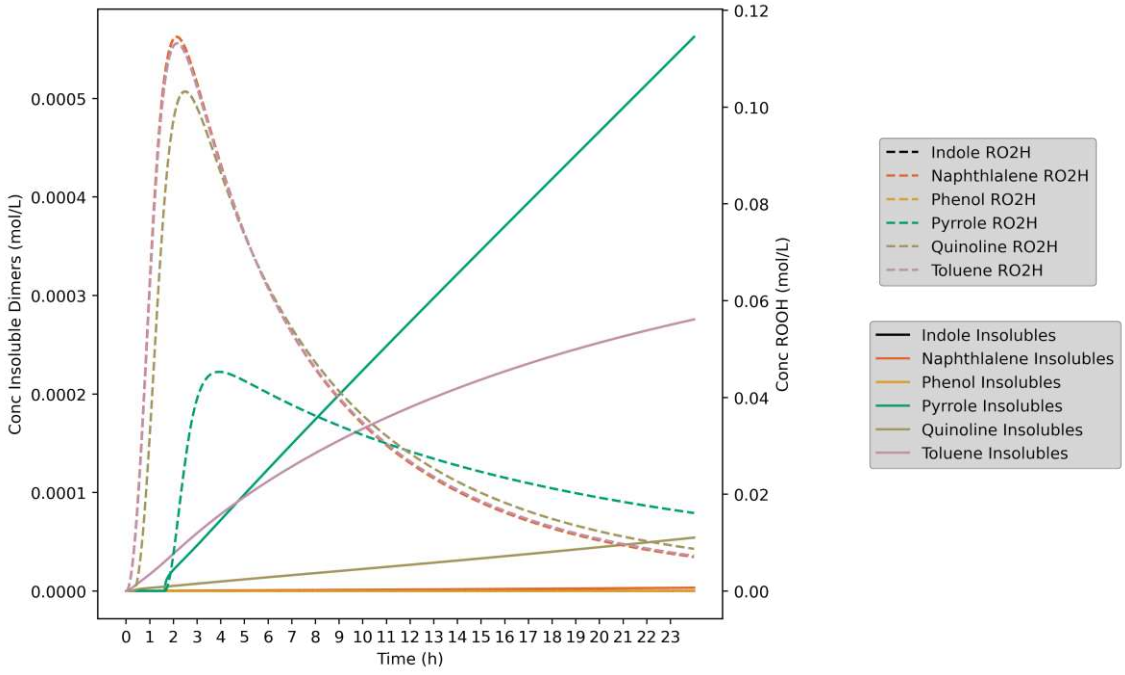

Figure 3.10: Change in the concentration of insolubles and ROOH over the course of the 24h pseudo-detailed models. The thick lines show the change in insoluble dimer concentration, whereas the dotted lines show the change in ROOH concentration. The results clearly show that for each species, as ROOH is depleted, the level insolubles begin to increase.

3.4 Implication for Fuels

A key novel finding of this study is the role that HAS reactions can play in deposit formation. Additionally, the work here represents the first study to apply DFT calculations to deposition reactions to attempt to predict deposition tendency from first principles.

One weakness of this study is that it looked solely into aromatic self-reactions via the HAS process, whereas side reactions between ArH and RH species will be dominant in a

real fuel scenario due to the low concentration of ArH in real-fuels. To briefly explore side reactions, we calculated the initial step of a HAS pathway between propanal, and various nitrogen compounds which is presented in Figure S.5 of the SI. In this pathway, propanal readily forms a σ-intermediate with the nitrogen heteroatoms. Future studies should explore the HAS pathway for fuel-aromatic side reactions, particularly as no mechanism is currently proposed in the fuel literature which does not rely on a termination step to form the C-C bond or without unrealistic EAS steps forming charged intermediates.[52]

The formation of fuel insolubles is influenced by both the H-abstraction and coupling propensity of the heteroatoms/aromatics present in fuel. By simplifying the insoluble formation process into the formation of dimers, we were able to show clear differences between the insoluble formation and antioxidant tendency between surrogate fuels. Nevertheless, the formation of dimers represents a small subsection of the insoluble/deposit structure. To expand the mechanism to reach an insolubles formation model which can provide a quantitatively accurate description, additional pathways need to be considered. This is a challenge, particularly as there are likely thousands of possible side reactions between and within species classes.[2] Even in our surrogate fuels the oxidation of *n*-dodecane is not significantly repressed.

To address the challenge of building a branching deposition mechanism with thousands of reactions, several approaches using techniques benchmarked in this study can be used. The first approach involves scaling the deposit forming dimer steps to experimental deposit measurements. This would lead to a semi-empirical mechanism, which moves away from the first-principles approach using DFT. Nevertheless, the DFT

thermochemical and kinetic parameters will allow the gross differences between species class and structure to be explored. This approach relies on the assumption that the formation of deposit dimers relates to a general property of 'coupling propensity'. Some preliminary calculations imply this assumption is generally correct, where a propanal doublet attacking various nitrogen compounds give barrier sizes (presented in Figure S.5 in the SI) in the same order of magnitude as the dimerization barriers for step B) in Figure 3.5.

A second, more computationally intensive approach, would be a set of high throughput calculations on additional deposit forming pathways. This approach would use HAS and termination reactions to calculate the pathways to various oligomers. These reactions could be constructed following chemical graph theory, as employed in recent work with phenols.[53] Hansen solubility parameters will guide a 'cut-off' point for energetic pathways to oligomers to form insolubles. Nevertheless, insoluble species are still likely to react to form larger molecular weight species, which adds an additional challenge to this approach.

Declaration of Interest

This research was partly funded by the University of Sheffield Department of Mechanical Engineering, PhD Scholarship Scheme, and the Powerplant Integration of Novel Engine Systems (PINES) grant number 113263.

4.5 Conclusions

The formation of insolubles in fuel is driven by coupling reactions between aromatics. In this work we have shown the importance of HAS in explaining the formation of these

insolubles. DFT calculations revealed that the hydroperoxides play a key role in facilitating the HAS pathway. As a result of these findings, we showed that kinetic values calculated for a simplified two-component (dodecane and aromatic) surrogate can reveal differences in antioxidant and deposition tendency of different aromatics compared to the experiment. In addition, when the HAS pathway is excluded, the predicted deposition trends break down. Exploring the behavior of the mechanism further, we show that the addition of antioxidant to an antioxidant+aromatic model leads the suppression of insolubles composed of the aromatic. Instead, the antioxidant+aromatic model leads to insolubles only composed of the antioxidant. Finally, sensitivity analysis reveals that the formation of hydroperoxides ($ArH + ROO \rightarrow Ar\cdot + ROOH$) and the homolytic coupling ($ArH + Ar\cdot \rightarrow ArHAr\cdot$) have a strong influence on the final deposit mass.

BIBLIOGRAPHY

1- T. Jia, L. Pan, S. Gong, J. Xie, X. Wang, Y. Fang, J. J. Zou, and X. Zhang, "Mechanistic insights into the thermal deposition of highly thermal-stable jet fuel," *Fuel*, vol. 276, no. May, p. 118100, 2020.

2- M. Commodo, I. Fabris, C. P. T. Groth, and Ö. L. Gülder, "Analysis of aviation fuel thermal oxidative stability by electrospray ionization mass spectrometry (ESI-MS)," *Energy and Fuels*, vol. 25, no. 5, pp. 2142–2150, 2011.

3- S. P. Heneghan and S. Zabarnick, "Oxidation of jet fuels and the formation of deposit," *Fuel*, vol. 73, pp. 35–43, jan 1994.

4- F. R. Mayo and B. Y. Lan, "Gum and deposit formation from jet turbine and diesel fuels at 130.degree.C," *Industrial Engineering Chemistry Product Research and Development*, vol. 25, pp. 333–348, jun 1986.

5- N. J. Kuprowicz, S. Zabarnick, Z. J. West, and J. S. Ervin, “Use of measured species class concentrations with chemical kinetic modeling for the prediction of autoxidation and deposition of jet fuels,” *Energy and Fuels*, vol. 21, no. 2, pp. 530–544, 2007.

6- R. H. Clark and L. Smith, “Further studies of the effects of polar compounds on the thermal stability of jet fuel,” in *3rd International Conference on Stability And Handling of Liquid Fuels*, no. 2, 1988.

7- S. Zabarnick, Z. J. West, L. M. Shafer, S. S. Mueller, R. C. Striebich, and P. J. Wrzesinski, “Studies of the role of heteroatomic species in jet fuel thermal stability: model fuel mixtures and real fuels,” *Energy and Fuels*, vol. 33, no. 9, pp. 8557–8565, 2019.

8- L. M. Balster, S. Zabarnick, R. C. Striebich, L. M. Shafer, and Z. J. West, “Analysis of polar species in jet fuel and determination of their role in autoxidative deposit formation,” *Energy and Fuels*, vol. 20, no. 6, pp. 2564–2571, 2006.

9- M. Grzybowski, K. Skonieczny, H. Butenschön, and D. T. Gryko, “Comparison of oxidative aromatic coupling and the scholl reaction,” *Angewandte Chemie - International Edition*, vol. 52, no. 38, pp. 9900–9930, 2013.

10- P. D. McDonald and G. A. Hamilton, *Mechanisms of Phenolic Oxidative Coupling Reactions*, vol. 5. Academic Press, INC., 1973.

11- W. R. Bowman and J. M. Storey, “Synthesis using aromatic homolytic substitution—recent advances,” *Chemical Society Reviews*, vol. 36, no. 11, pp. 1803–1822, 2007.

12- C.-L. Sun and Z.-J. Shi, “Transition-metal-free coupling reactions,” *Chemical Reviews*, vol. 114, no. 18, pp. 9219–9280, 2014. PMID: 25184859.

13- M. Monge-Palacios, E. Grajales-González, G. Kukkadapu, and S. M. Sarathy, “Kinetics of the benzyl + HO2and benzoxyl + OH barrierless association reactions: fate of the benzyl hydroperoxide adduct under combustion and atmospheric conditions,” *Physical Chemistry Chemical Physics*, vol. 22, no. 16, pp. 9029–9039, 2020.

14- F. Minisci, “Recent aspects of homolytic aromatic substitutions.,” *Topics in current chemistry*, vol. 62, pp. 1–48, 1976.

15- B. Beaver, L. Gao, C. Burgess-Clifford, and M. Sobkowiak, “On the mechanisms of formation of thermal oxidative deposits in jet fuels. Are unified mechanisms possible for both storage and thermal oxidative deposit formation for middle distillate fuels?,” *Energy and Fuels*, vol. 19, no. 4, pp. 1574–1579, 2005.

16- T. Stuyver, D. Danovich, F. De Proft, and S. Shaik, “Electrophilic Aromatic Substitution Reactions: Mechanistic Landscape, Electrostatic and ElectricField

642 Control of Reaction Rates, and Mechanistic Crossovers," *Journal of the*
643 *American Chemical Society*, vol. 141, no. 24, pp. 9719–9730, 2019.

644 17- D. P. Curran and A. I. Keller, "Radical additions of aryl iodides to arenes are
645 facilitated by oxidative rearomatization with dioxygen," *Journal of the*
646 *American Chemical Society*, vol. 128, no. 42, pp. 13706–13707, 2006.

647 18- R. Venkataraman and S. Eser, "Characterisation of solid deposits from the
648 thermal-oxidative degradation of jet fuel," *International Journal of Oil, Gas*
649 *and Coal Technology*, vol. 1, no. 1-2, pp. 126–137, 2008.

650 19- O. Altin and S. Eser, "Carbon deposition from thermal stressing of petroleum
651 fuels," *ACS National Meeting Book of Abstracts*, vol. 228, no. 1, 2004.

652 20- Z. Liu, S. Tang, Z. Li, Z. Qin, S. Yuan, L. Wang, L. Wang, X. Zhang, and G.
653 Liu, "An improved kinetic model for deposition by thermal oxidation of
654 aviation hydrocarbon fuels," *Fuel*, vol. 258, no. June, p. 116139, 2019.

655 21- C. M. Parks, A. J. Meijer, S. G. Blakey, E. Alborzi, and M. Pourkashanian,
656 "Computational studies on the reactions of thiols, sulfides and disulfides with
657 hydroperoxides. Relevance for jet fuel autoxidation," *Fuel*, vol. 316, no.
658 January, p. 123326, 2022.

659 22- E. Alborzi, M. R. Dwyer, C. M. , A. Sheikhansari, D. C. Mielczarek, M.
660 Zanganeh, A. J. Meijer, S. G. Blakey, and M. Pourkashanian, "Construction of

a reduced chemical kinetic mechanism for autoxidation of n-paraffinic solvent – A model for aviation fuel," *Fuel*, vol. 294, no. January, p. 120170, 2021.

23- A. C. Antoine, "EFFECT OF SOME NITROGEN COMPOUNDS ON THERMAL STABILITY OF JET A.," *NASA Technical Memorandum*, jun 1982.

24- L. Jones and N. C. Li, "Ageing of SRC II middle distillate from Illinois No. 6 coal," *Fuel*, vol. 62, no. 10, pp. 1156–1160, 1983.

25- R. N. Hazlett and A. J. Power, "Phenolic compounds in Bass Strait distillate fuels: their effect on deposit formation," *Fuel*, vol. 68, no. 9, pp. 1112–1117, 1989.

26- T. Jia, M. Zhao, L. Pan, C. Deng, J.-j. Zou, and X. Zhang, "Effect of phenolic antioxidants on the thermal oxidation stability of high-energy-density fuel," *Chemical Engineering Science*, p. 117056, 2021.

27- John M. Andrésen, James J. Strohm, , Lu Sun, and C. Song*, "Relationship between the Formation of Aromatic Compounds and Solid Deposition during Thermal Degradation of Jet Fuels in the Pyrolytic Regime," 2001.

28- S. Jain and M. P. Sharma, "Review of different test methods for the evaluation of stability of biodiesel," *Renewable and Sustainable Energy Reviews*, vol. 14, no. 7, pp. 1937–1947, 2010.

29- M. J. Frisch, G. W. Trucks, H. B. Schlegel, G. E. Scuseria, M. A. Robb, J. R. Cheeseman, G. Scalmani, V. Barone, B. Mennucci, G. A. Petersson, H. Nakatsuji, M. Caricato, X. Li, H. P. Hratchian, A. F. Izmaylov, J. Bloino, G. Zheng, J. L. Sonnenberg, M. Hada, M. Ehara, K. Toyota, R. Fukuda, J. Hasegawa, M. Ishida, T. Nakajima, Y. Honda, O. Kitao, H. Nakai, T. Vreven, J. A. Montgomery, Jr., J. E. Peralta, F. Ogliaro, M. Bearpark, J. J. Heyd, E. Brothers, K. N. Kudin, V. N. Staroverov, R. Kobayashi, J. Normand, K. Raghavachari, A. Rendell, J. C. Burant, S. S. Iyengar, J. Tomasi, M. Cossi, N. Rega, J. M. Millam, M. Klene, J. E. Knox, J. B. Cross, V. Bakken, C. Adamo, J. Jaramillo, R. Gomperts, R. E. Stratmann, O. Yazyev, A. J. Austin, R. Cammi, C. Pomelli, J. W. Ochterski, R. L. Martin, K. Morokuma, V. G. Zakrzewski, G. A. Voth, P. Salvador, J. J. Dannenberg, S. Dapprich, A. D. Daniels, Ö. Farkas, J. B. Foresman, J. V. Ortiz, J. Cioslowski, and D. J. Fox, "Gaussian 09 Revision E.01," 2009. Gaussian Inc. Wallingford CT 2009.

30- A. D. Becke, "Density-functional thermochemistry. III. The role of exact exchange," *The Journal of Chemical Physics*, vol. 98, no. 7, pp. 5648–5652, 1993.

31- S. Grimme, S. Ehrlich, and L. Goerigk, "Effect of the damping function in dispersion corrected density functional theory," *Journal of computational chemistry*, vol. 32, no. 7, pp. 1456–1465, 2011.

32- S. Miertuš, E. Scrocco, and J. Tomasi, “Electrostatic interaction of a solute with a continuum. a direct utilizaion of ab initio molecular potentials for the prevision of solvent effects,” *Chemical Physics*, vol. 55, no. 1, pp. 117–129, 1981.

33- T. H. Dunning Jr, “Gaussian basis sets for use in correlated molecular calculations. i. the atoms boron through neon and hydrogen,” *The Journal of chemical physics*, vol. 90, no. 2, pp. 1007–1023, 1989.

34- S. Grimme, “Supramolecular binding thermodynamics by dispersion-corrected density functional theory,” *Chemistry–A European Journal*, vol. 18, no. 32, pp. 9955–9964, 2012.

35- R. F. Ribeiro, A. V. Marenich, C. J. Cramer, and D. G. Truhlar, “Use of solution-phase vibrational frequencies in continuum models for the free energy of solvation,” *The Journal of Physical Chemistry B*, vol. 115, no. 49, pp. 14556–14562, 2011.

36- R. Paton, “Goodvibes,” 2016.

37- S. Zabarnick, “Chemical kinetic modeling of jet fuel autoxidation and antioxidant chemistry,” *Industrial Engineering Chemistry Research*, vol. 32, pp. 1012–1017, jun 1993.

718 38- S. Kobayashi and H. Higashimura, “Oxidative polymerization of phenols
719 revisited,” *Progress in Polymer Science (Oxford)*, vol. 28, no. 6, pp. 1015–
720 1048, 2003.

721 39- S. Baena-Zambrana, S. L. Repetto, C. P. Lawson, and J. K. Lam, “Behaviour
722 of water in jet fuel - A literature review,” *Progress in Aerospace Sciences*, vol.
723 60, pp. 35–44, 2013.

724 40- J. K. Howard, K. J. Rihak, A. C. Bissember, and J. A. Smith, “The Oxidation
725 of Pyrrole,” *Chemistry - An Asian Journal*, vol. 11, no. 2, pp. 155–167, 2016.

726 41- Z. Zhang, X. Yue, Y. Duan, and Z. Rao, “A study on the mechanism of oxidized
727 quinoline removal from acid solutions based on persulfate-iron systems,” *RSC*
728 *Advances*, vol. 10, no. 21, pp. 12504–12510, 2020.

729 42- J. D. Mosley, A. M. Ricks, P. V. Schleyer, J. I. Wu, and M. A. Duncan, “IR
730 spectroscopy of ↵- And -protonated pyrrole via argon complex
731 photodissociation,” *Journal of Physical Chemistry A*, vol. 116, no. 39, pp.
732 9689–9695, 2012.

733 43- M. J. DeWitt, Z. West, S. Zabarnick, L. Shafer, R. Striebich, A. Higgins, and
734 T. Edwards, “Effect of Aromatics on the Thermal-Oxidative Stability of
735 Synthetic Paraffinic Kerosene,” *Energy & Fuels*, vol. 28, pp. 3696–3703, jun
736 2014.

44- S. Zabarnick, “Chemical kinetic modeling of jet fuel autoxidation and antioxidant chemistry,” *Industrial Engineering Chemistry Research*, vol. 32, pp. 1012–1017, jun 1993.

45- . Wang, A. Violi, D. H. Kim, and J. A. Mullholland, “Formation of naphthalene, indene, and benzene from cyclopentadiene pyrolysis: A DFT study,” *Journal of Physical Chemistry A*, vol. 110, no. 14, pp. 4719–4725, 2006.

46- Zotti, G., Zecchin, S., Schiavon, G., Seraglia, R., Berlin, A., & Canavesi, A. (1994). Structure of Polyindoles from Anodic Coupling of Indoles: An Electrochemical Approach. Chemistry of Materials, 6(10), 1742–1748. https://doi.org/10.1021/cm00046a029 P. J. Steel, “Aromatic biheterocycles: Syntheses, structures, and properties,” *Advances in heterocyclic chemistry*, vol. 67, pp. 2–118, 1997.

47- Talbi, H., Monard, G., Loos, M., & Billaud, D. (1998). Theoretical study of indole polymerization. Journal of Molecular Structure: THEOCHEM, 434(1–3), 129–134. https://doi.org/10.1016/S0166-1280(98)00092-X

48- R. N. Hazlett, J. A. Schreifels, W. M. Stalick, R. E. Morris, and G. W. Mushrush, “Distillate fuel insolubles: formation conditions and characterization,” *Energy and Fuels*, vol. 5, no. 2, pp. 269–273, 1991.

49- Z., Steven, P. Zelesnik, and P. R. Grinstead. "Jet fuel deposition and oxidation: dilution, materials, oxygen, and temperature effects." *Turbo Expo: Power for*

Land, Sea, and Air. Vol. 78804. American Society of Mechanical Engineers, 1995.

50- Hazlett, R. N. (1991). Thermal Oxidation Stability of Aviation Turbine Fuels. In Thermal Oxidation Stability of Aviation Turbine Fuels. https://doi.org/10.1520/mono1-eb

51- Liu, S., Zhao, F., Chen, X., Deng, G. J., & Huang, H. (2020). Aerobic Oxidative Functionalization of Indoles. Advanced Synthesis and Catalysis, 362(18), 3795–3823. https://doi.org/10.1002/adsc.202000285

52- Adams, C., Alborzi, E., Meijer, A. J. H. M., Hughes, K. J., & Pourkashanian, M. (2023). Mechanistic investigation into the formation of insolubles in bulk fuel jet fuel using quantum chemical and experimental techniques. Fuel, 334(P1), 126202. https://doi.org/10.1016/j.fuel.2022.126202

53- Raza, Z., Naz, K., & Ahmad, S. (2022). Expected Values of Molecular Descriptors in Random Polyphenyl Chains. Emerging Science Journal, 6(1), 151–165. https://doi.org/10.28991/ESJ-2022-06-01-012

EXPLORING HOMOLYTIC AROMATIC SUBSTITUTION AS A DRIVER FOR FUEL DEPOSITION WITH QUANTUM CHEMISTRY AND EXPERIMENTS

Charlie Adams,[*,†] Marco Conte,[‡] Ehsan Alborzi,[*,†] Anthony JHM Meijer,[†] Kevin Hughes,[†] and Mohamed Pourkashanian [*,†]

†*Department of Mechanical Engineering, The University of Sheffield, Sheffield, S3 7RD, UK* ‡*Department of Chemistry, The University of Sheffield, Sheffield, S3 7RD, UK*

E-mail: cadams2@sheffield.ac.uk; e.alborzi@sheffield.ac.uk; mohamed.pourkashanian@sheffield.ac.uk

Abstract

Liquid phase insoluble formation in fuels can cause performance and safety issues. To understand the formation of insolubles in fuels from first principles, a series of density functional theory (DFT) calculations were run to calculate the energetic barriers of the autoxidation and coupling reactions for several common fuel aromatics/heteroatoms. The six compounds chosen were phenol, toluene, naphthalene, pyrrole, quinoline, and indole. Using a combination of DFT calculations and gravimetric and petroxy experimental work, a novel homolytic aromatic substitution (HAS) coupling pathway was identified for each compound. While previous studies have treated deposition steps implicitly, our detailed calculations of HAS reactions and bulk fuel (RH) oxidation reaction barriers afforded the development of

bespoke pseudo-detailed mechanisms for each aromatic compound with explicit reaction steps. These mechanisms were then used to predict trends in deposition behavior of the compounds tested in a simple n-dodecane surrogate. The novel HAS mechanism suggested for fuels was proposed to start with the reaction of an aromatic radical (Ar·) to an aromatic (ArH), which then formed a radical (ArHAr·) σ-intermediate. It was then found that hydroperoxides (ROOH) could re-aromatize the radical intermediate (ArHA·), forming a deposit dimer (ArAr). Although our sensitivity analysis revealed that alkyl fuel radical and fuek alkoxyl radical abstraction steps influenced the final mass of the deposit, the Ar.+ArH HAS coupling step was found to have the largest influence. Finally, an aromatic/heteratom model containing phenol and toluene was built, which showed that phenol suppressed deposition from toluene, and peaked in deposit mass at a phenol:toluene ratio of 25:75. Although our study was limited to Ar self-reactions, we hypothesize that bulk fuel – aromatic coupling could also be governed by HAS reactions, allowing researchers to move towards a more first-principles based deposition model.

Keywords: Density Functional Theory, Homolytic Aromatic Substitution, Thermal Stability, Jet Fuel, Pseudo-detailed Mechanism

1. Introduction

The formation of insolubles in the liquid-phase of jet fuels is mainly driven by the formation of oligomers from fuel components.[1, 2] Oligomers successively grow starting from dimers, trimers, tetramers and so on. Each oligomer growth step is predominantly characterized by the formation of C–C and C–O bonds. Previous research has emphasized the termination of antioxidant and/or fuel components ($Ar\cdot + Ar\cdot \rightarrow Ar_2$) as a key source of fuel insolubles, and by that extension C–C/C–O bond formation.[3, 4, 5] This has led Heneghan and

Zabarnick to highlight an inverse correlation between the ease of oxidation and the formation of deposits. In other words, a fuel with a lower oxidation rate arises from the higher concentration of chain-breaking Ar· radicals, and therefore have a higher concentration of Ar· to undergo termination steps producing deposit.[3] However, in some instances, this relation does not always hold. Notably, some nitrogen compounds like pyrroles and indoles tend to show low/no effects on autoxidation rates yet are severe deposit promoters.[6, 7, 8] To explain these exceptions, Heneghan and Zabarnick propose that some fuels produce termination Ar–Ar products with a higher solubility.[3] Nevertheless, there may be other chemical factors that need to be explored.

The formation of Ar–Ar via the termination of two free-radicals Ar· in solution is part of an oxidative coupling process. However, it is possible to form Ar–Ar without a termination step under oxidative conditions. Focusing on transition metal free processes, homolytic aromatic substition (HAS) has received considerable attention as a method for cross-coupling aromatic compounds under free-radical conditions.[9, 10, 11, 12] Additionally, HAS mechanisms have been used as a way to understand the rate of radical reactions.[13, 14] The general mechanism of HAS is shown in Figure 1.1. First, an attack of an aryl radical to an arene compound generates a σ-intermediate. The σ-intermediate is then re-aromatized via elimination of a leaving group forming a dimer. In this sense, HAS reactions are analogous to electrophilic aromatic substitution (EAS) reactions, except that the σ-intermediate is not charged. EAS reactions have been proposed as a mechanism in the formation of jet fuel deposits.[15] However, in aprotic non-polar jet fuel, the stabilization of charged EAS σ-intermediates is precluded.[16] By contrast, HAS reactions have been shown to readily occur in non-polar aprotic solvents between arenes under molecular oxygen.[17] In general HAS reactions have presented a challenge to organic chemists due to poor selectivity, leading to intractable mixtures.[11] Nevertheless, in the context of jet fuel fouling, fuel deposits and

gums are characterized by highly disordered coupled products composed of mainly aromatic groups.[18, 19] Overall, the HAS reactions between aromatic fuel species should be investigated as possible route to deposits. Particularly as HAS offers a route to form C–C bonds without terminating the free-radical chain mechanism, and can instead be considered a propagation step.

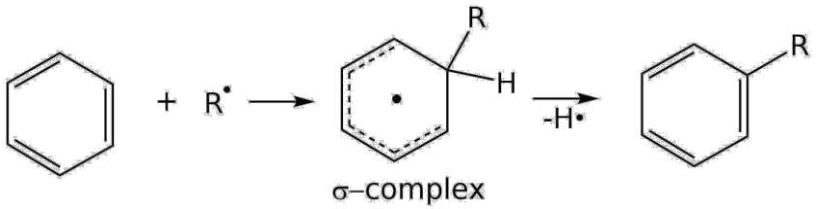

Figure 1.1: Generalized HAS mechanism, where an Ar· radical attacks a generic aromatic species. This attack subsequently forms a sigma-complex, which is in a doublet state. The sigma complex is re-aromatized by the loss of a hydrogen *via* an unspecified mechanism.

Several reactions for the formation of insolubles/deposits are represented in pseudo-detailed mechanisms in the public literature.[5, 20] However, at present, they are implicit. As a result, they do not represent specific chemical transformations, but are composed of 'pseudo' species with parameters fitted to experiments. In the future, a wider range of fuel chemistries and blends will require predictive mechanisms with greater sensitivity to the starting components, without relying too heavily on fitting parameters. However, due to complexity and range of insoluble structures, a compromise needs to be met between the range of reactions and products represented.

In recent years, density functional theory (DFT) has become a popular tool to build pseudo-detailed mechanisms jet fuel deposition from 'first-principles'.[21, 22] DFT allows direct calculations of thermochemical and kinetic data, and evaluation of competing chemical reaction pathways. By contrast, previous pseudo-detailed mechanisms have been produced by producing activation energies from fitted experimental data.[5, 20] However, this leads to mechanisms which are only suitable for specific types of fuel.

It is the aim of this paper to: 1) explore the possibility of HAS as a route to insolubles formation and 2) attempt to predict insoluble formation tendencies using DFT methods. First, several two-component fuels containing bulk and heteroatoms will be stressed to produce an insoluble mass. Then, the energetic pathways from fuel heteroatoms and bulk species to dimers are calculated and compared to insolubles generated by the surrogate fuels. As a means of understanding the deposition process further, the solubility of oligomers will be considered too.

2 Methods and Materials

2.1 Surrogate Fuels for this Study

Six surrogate fuels were built with a range of compounds designed to represent the different heteroatom and aromatic compounds found in fuels. Out of the nitrogen class of compounds pyrrole (Sigma Aldrich, >98% purity), quinoline (Oakwood chemicals, >98% purity), and indole (Sigma Aldrich, >99% purity) were selected.

Pyrrole and indole are two 5-membered nitrogen heteratom compounds known to promote insoluble formation, with pyrrole being a particularly problematic insoluble promoter.[8, 23] Quinoline has been shown to also promote insolubles, but to a lesser degree than pyrrole and

indole.[8, 7] Next, phenol (ACROS Organics, >99%) was chosen to represent the phenolic class of compounds, again shown to promote insolubles in a variety of real and surrogate fuels.[8, 24, 25, 26] Finally, two aromatic components, naphthalene (Fluorochem, >99%) and toluene (SLS, 99.5%) were chosen for their presence in the mono-aromatic and di-aromatic class in fuels.[27] Each of the above six components were added as 0.1 mol l^{-1} to *n*-dodecane (ACROS Organics, >99%).

The authors acknowledge that the chosen concentration of 0.1 mol l^{-1}, equivalent to approximately 20,000 ppm of aromatics, is significantly higher than the heteroatom levels typically found in real fuels, which generally range from 100 to 1000 ppm.[51] However, even at this high concentration, the amount of deposit generated from 5 ml of surrogate fuel is relatively low. Therefore, the fuel needed to be spiked with this level of deposit for the study given the sensitivity of the deposit measurement equipment. Furthermore, the primary focus of this study was to investigate the coupling between aromatics in the presence of hydrogen abstraction and addition reactions, hence the requirement for a high concentration of aromatic species to ensure dominant Ar-Ar reactions. Nevertheless, in a real fuel scenario, fuel-aromatic reactions would likely be more prevalent. While homolytic aromatic substitutions would still be relevant (including for fuel-Ar reactions), their impact on the coupling reactions between different species would be more challenging to examine due to the increased complexity of coupling pathways.[14]

Another aspect of the design of the surrogate fuels in this study which differ from real fuels was the selection of unsubstituted aromatics. Real fuel aromatics have multiple alkyl-substitutions round the ring aromatic ring. We chose to investigate unsubstituted compounds as a ‘base-case’ for the coupling reactions here. This base-case was chosen here such that gross differences in aromatic classes could be explored. Future studies adding substituted

groups would add another dimension to the work, where the effect of substitutions *within and between* each compound class could be explored. Moving beyond the base-case towards a more realistic fuel molecule, additional alkyl- substitutions would likely have two effects based on EAS and HAS theory: 1) block reactive sites where alkyl- substitutions are present and 2) act as weak directing groups.[11] Thes is also the possibility that alkyl-substitutions would affect the solubility, which can be explored in future work via the methods detailed in section 2.2.

2.2 Method of Thermal Stressing and Deposit Measurement

To produce the insoluble masses, 5 ml of fuel was added to a 50 ml borosilicate round bottom pressurized flask. The flask was heated to 140°C for 24 h under 1 bar constant oxygen supply. The flask was sealed to all gases aside from the supplied oxygen. After heating, the flask was allowed to cool and insolubles were then filtered through a 0.1 µm glass fibre filter to give the total weight of insolubles in the bulk. The flask was then washed with trisolvent and then washed into a flask. The flask was then dried in a vacuum oven to remove any liquid residue, weighed, and then compared with the weight of the clean flask- giving the total weight of adherent insolubles left in the flask.[28] The sum of the insolubles weights on the filter and in the flask gave a mass total insolubles per surrogate. The deposit experiments were repeated at least 3 times for each surrogate to improve the accuracy of the total insolubles measurement.

A petroOxy device was used to produce oxygen depletion curves for each surrogate fuel. The petroOxy device is a sealed gold-lined chamber in which 5 ml of fuel is thermally

stressed at 140°C. The headspace above the heated fuel is depleted as the fuel is stressed, giving a measure of the rate of oxygen consumption in the bulk fuel.

2.3 Hansen Solubility Parameters and Computational Details

All calculations were performed in Gaussian09 (E.01) using the B3LYP functional.[29][30] Grimme's DFT-D3(BJ) dispersion correction was applied to all the calculations to account for long-range effects.[31] A PCM solvation model, with n-dodecane as the chosen solvent, was selected to replicate the hydrocarbon bulk.[32] The basis set chosen was cc-pVTZ on an ultrafine grid. This basis set adds polarization functions, allowing orbital hybridization to be taken into account.[33] Transition states were optimized using the QST1/3 method depending on the reaction studied. All transitions states were verified by the presence of one imaginary frequency corresponding to the saddle point. Additionally, intrinsic reaction coordinate (IRC) calculations were performed to verify the transition state corresponded to the expected reactants and products. Unrestricted (broken symmetry) calculations were performed on open-shell systems, where the HOMO and LUMO were mixed (guess=mix option). Entropy values were corrected using the GoodVibes script, which employs a quasi-harmonic correction corrected at 298K.[34, 35, 36]

In Hansen solubility theory, three Hansen solubility parameters (HSPs) are assigned to each molecule: D for dispersion, P for polarity, and H for hydrogen bonding. As a consequence, each solvent exists in a 3-dimensional space of HSPs. The HSP distance between two molecules in the 3d HSP space is given by:

$$Ra^2 = 4(D_1 - D_2)^2 + (P_1 - P_2)^2 + (H_1 - H_2)^2 \quad (1.1)$$

Where R_a is the Hansen distance.

The HSP parameters for the test solvents were either obtained from the HSPIP dataset or calculated using the software. The HSPIP software requires a series of test solvents/solutes, tested for their solubility in the *n*-dodecane. A score 0 is assigned to insoluble solvents and a score of 1 is assigned to soluble solvents.

In each case, 0.1 mol l^{-1} of each test compound was added to 5ml of *n*-dodecane. Resulting from the series of tests is a 'sphere' in 3d HSP space, whose dimensions are determined by the solubility of the sphere (Figures 2.1 and 2.2). The radius of sphere R_0 is then used to asses the solubility of a proposed solvent, where R_a of the test molecule is used in the following equation:

$$RED = R_a/R_0. \quad (10.2)$$

Where RED stands for Relative Energy Difference. A RED > 1 implies the molecule is likely insoluble in your main solvent (*n*-dodecane in this case), whereas a RED < 1 implies the molecule is soluble. Our calculated sphere was composed of 13 lab grade compounds known for their presence in fuel and gave a fit of 1 according to HSPIP software. The results for these tests are presented in Table 2.1 . Here it is important to acknowledge that the solubility of the deposit precursors in pure *n*-dodecane this study will likely be different to a conventional fuel due to the presence of aromatic compounds and minor components. Nevertheless, these parameters are useful to understand insoluble formation our surrogate fuel, and to improve the HSP method for future studies.

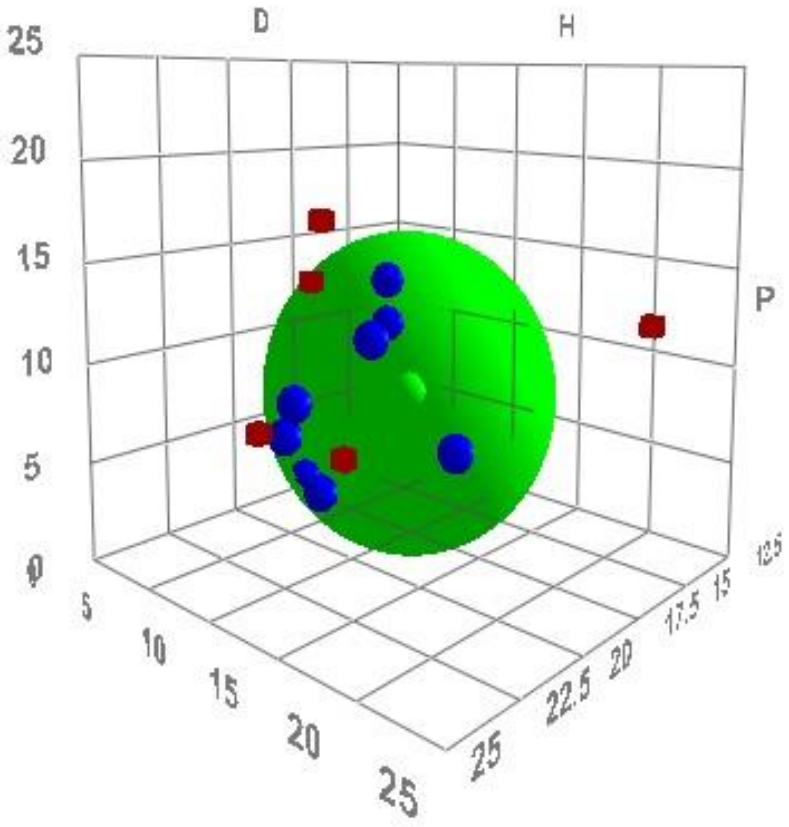

Figure 2.1: HSPIP Sphere

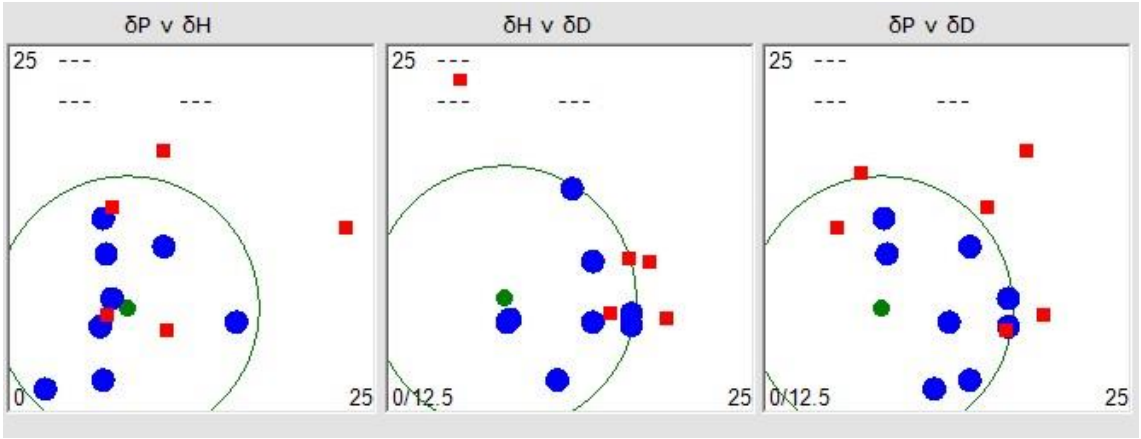

Figure 2.2: HSPIP Sphere parameter fits

Table 2.1: Hansen Solubility test solvents and their Associated HSPs. The sphere gave a fit of 1.000

Solvent	Database/Calculated HSP	D	P	H	Score	RED
Indigo	Calculated	21.10	17.4	10.0	0	1.639
Carbazole	Database	21.7	6.4	6.2	0	1.243
p-Benzoquinone	Database	19.8	13.7	6.5	0	1.121
Water	Database	15.5	16.0	42.3	0	4.042
2-Naphthol	Database	20.4	5.4	10.2	0	1.000
Methanol	Database	14.7	12.3	22.3	0	1.800
Di-*n*-Butyl Sulfoxide	Database	16.4	10.5	6.1	1	0.443
Naphthalene	Database	19.2	2.0	5.9	1	0.884
Pyrrole	Database	19.2	11.0	10.0	1	0.863
Dipropyl Sulfone	Database	16.3	12.9	5.9	1	0.705
Toluene	Database	18.0	1.4	2.0	1	0.961
Indole	Database	20.5	7.5	6.5	1	0.973
Phenol	Database	18.5	5.9	14.9	1	0.979
Quinoline	Database	20.5	5.6	5.7	1	0.995

2.4 Pseudo-Detailed Mechanism in Fuels

In order to compare the total insolubles to the number of dimers predicted by DFT, several new reaction steps were proposed which will be elucidated in the results and discussion. To

capture the autoxidation reactions in the bulk, the basic autoxidation scheme (BAS) was used which gave good agreement with oxygen and hydroperoxide depletion with experiment. The BAS scheme was optimized for a range of C10-C14 hydrocarbons, whereby the thermochemical and kinetic parameters were obtained using *n*-dodecane as the model fuel. Further details of the BAS scheme can be found in reference.[22] To construct the mechanism, the Eyring equation was used, with A being formed from the calculated entropy barrier and E_a formed from the calculated enthalpy barrier. All the forward and reverse barriers were calculated from a stable pre-reaction and post-reaction complex.

For each surrogate fuel, different mechanisms were constructed to study oxygen depletion and deposit formation. For oxygen depletion, the level of oxygen was fixed at 1.8 mmol l^{-1}.[37] For the deposition mechanism, oxygen was removed as a limiting reagent (kept constant at 1.8 mmol l^{-1}) to reflect the continuous supply of oxygen in our deposit forming rig. The mechanism was integrated in MATLAB using the **ode45** solver. The mechanism gave a molar concentration of a dimer, which was then related to a mass via the molecular weight of the proposed dimer.

3 Results and Discussion

3.1 Homolytic Aromatic Substitution Mechanism

The key bottleneck in any HAS reaction is the re-aromatization and liberation of hydrogen from the σ-intermediate. The loss of H· in this step is not well understood. Nevertheless, one paper exploring HAS reactions between aryl iodides and arenes using oxygen as an oxidant, proposed a re-aromatization step involving oxygen this is shown as reaction 1) in Figure 3.1 Because hydroperoxides (ROOH) and oxygenated species like alcohols (ROH) form under

oxidative conditions in fuels, these were also considered as possible reagents to remove hydrogen from the σ-intermediate. ROOH reacting with the σ-intermediate is proposed to form RO· and H_2O, is shown as reaction 2) in Figure 3.1. ROH reacting with the σ-intermediate is proposed to form R· and H_2O, is shown as reaction 3) in Figure 3.1.

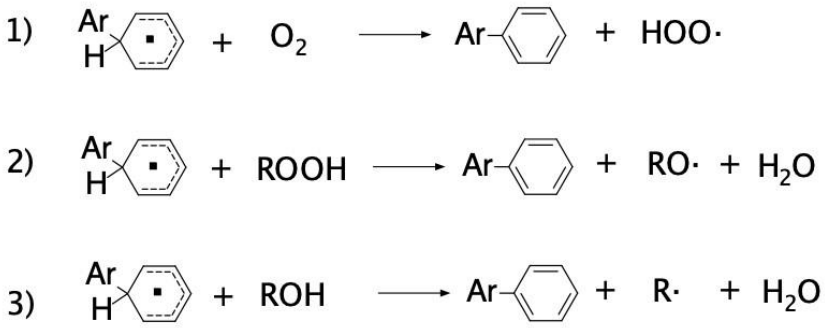

Figure 3.1: HAS reactions considered for fuel coupling reactions. Each step shows the σ-intermediate formed from an Ar· + ArH reaction, and the species chosen to re-aromatize the intermediate.

Considering the mechanisms presented in Figure 3.1, we explored the possibility of these reactions in phenolic coupling. Phenols have widely been recognized as being detrimental to fuel thermal stability.[8] HAS mechanisms have previously been considered as a possible pathway the oxidative coupling of phenols.[14] Nevertheless, it should be noted that in a real fuel, direct phenol-phenol coupling is not likely due to the concentration of phenolic compounds. However, the main of this section is to understand the possible re-aromatization step available to fuel species. The findings here will be used as a template for other fuel HAS reactions.

The calculated HAS pathways for phenol are presented in Figure 3.2. First, the formation of the σ-intermediate is endergonic and has a free-energy barrier of $^{\ddagger}G$=+25.64kcalmol ^{1} leading to an intermediate PhOPhO·. The para- position of the phenol was chosen as the site

of oxidative coupling of another phenoxy radical given that this is the generally the more favorable site.[38] The first mechanism in Figure 3.1, involving the re-aromatization with oxygen, could not be identified for phenol. A key challenge with the oxygen transition state is the choice of spin multiplicity. Given that oxygen is in the triplet state, and the system σ-intermediate is in the doublet state, an open-shell doublet or a quartet surface can be chosen.

The other two mechanisms presented in Figure 3.1 involve ROH and ROOH. The ROOH pathway in Figure 3.2 shows a lower barrier to re-aromatization of the intermediate compared to the ROH by 30.22 kcal mol^{-1}. Additionally, the ROOH is thermodynamically favored, namely due to the enhanced stability of the RO· radical compared to R· The IRCs for both these pathways are presented in Figures S.1 and S.2 in the SI. The ROOH and ROH re-aromatization transition states are characterized by a rotation of the terminal OH moiety towards an available hydrogen at the para-coupling site.

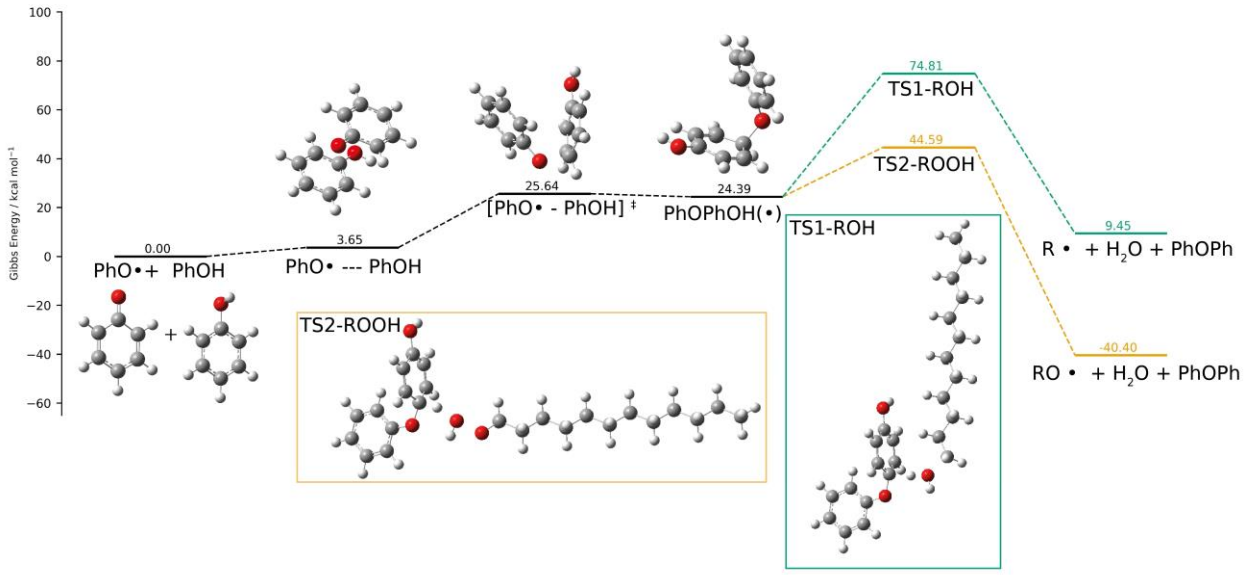

Figure 3.2: Comparison of different HAS pathways at the B3LYP-D3//cc-pVTZ level of theory using *n*-dodecane (PCM) as a solvent. The first step of the process in black shows the Ar· + ArH---ArHAr· reaction of a phenol and a phenoxy radical, leading to the σ-

intermediate. The subsequent levels in green shows the re-aromatization step with ROH and the level in orange shows the re-aromatization step with an ROOH species.

3.2 Comparison of Antioxidant Oligomer Solubility and Pathway to Deposit

To justify the assumption that the formation of insolubles results from the coupling of ArH species, we calculated Hansen solubility parameters for oligomers for our chosen heterotoms of increasing size. Previous research has hypothesized that aromatic compounds in fuel rapidly become insoluble as they grow in size.[43] Figure 3.3 shows the change in RED score as the oligomer chain grows, where relative energy difference (RED) > 1 indicates an oligomer that has become insoluble in *n*-dodecane. For real fuels, these results will vary, particularly as the aromatic content will increase the 'likeness' of the solvent to other extended aromatic structures.[39] Nevertheless, because our model fuels in this study contain *n*-dodecane as the base solvent, the Hansen plots here are a useful tool to explore deposition tendency in our model fuels. Oligomer structures were chosen based on the favored coupling site for each heteratom based on literature data and our calculations.[38, 40, 41, 42] The phenol chain growth is shown as an example. What is clear is that in general as the oligomer grows, the solubility in *n*-dodecane decreases. However, different oligomers reach the insolubility threshold in fewer units, where a single unit is the monomer, 2 units is a dimer and so on. For example, comparing toluene and naphthalene, naphthalene reaches the insolubility threshold after 2 units have coupled. This is consistent with previous observations that di-aromatics form deposit more rapidly because they 'require fewer consecutive reaction steps to produce high-molecular-weight'.[43]

Interestingly, heteroatom size does not influence the solubility of the resultant oligomers. Instead, the lower solubility is related to the dD parameter in the HAS framework, representing Van Der Waals forces between the solvent and heteroatom. As the oligomers grow, the difference in polarity and hydrogen bonding begins to decrease (indicated by the decreasing dP and dH parameters), but the difference in dispersion forces dD increases.

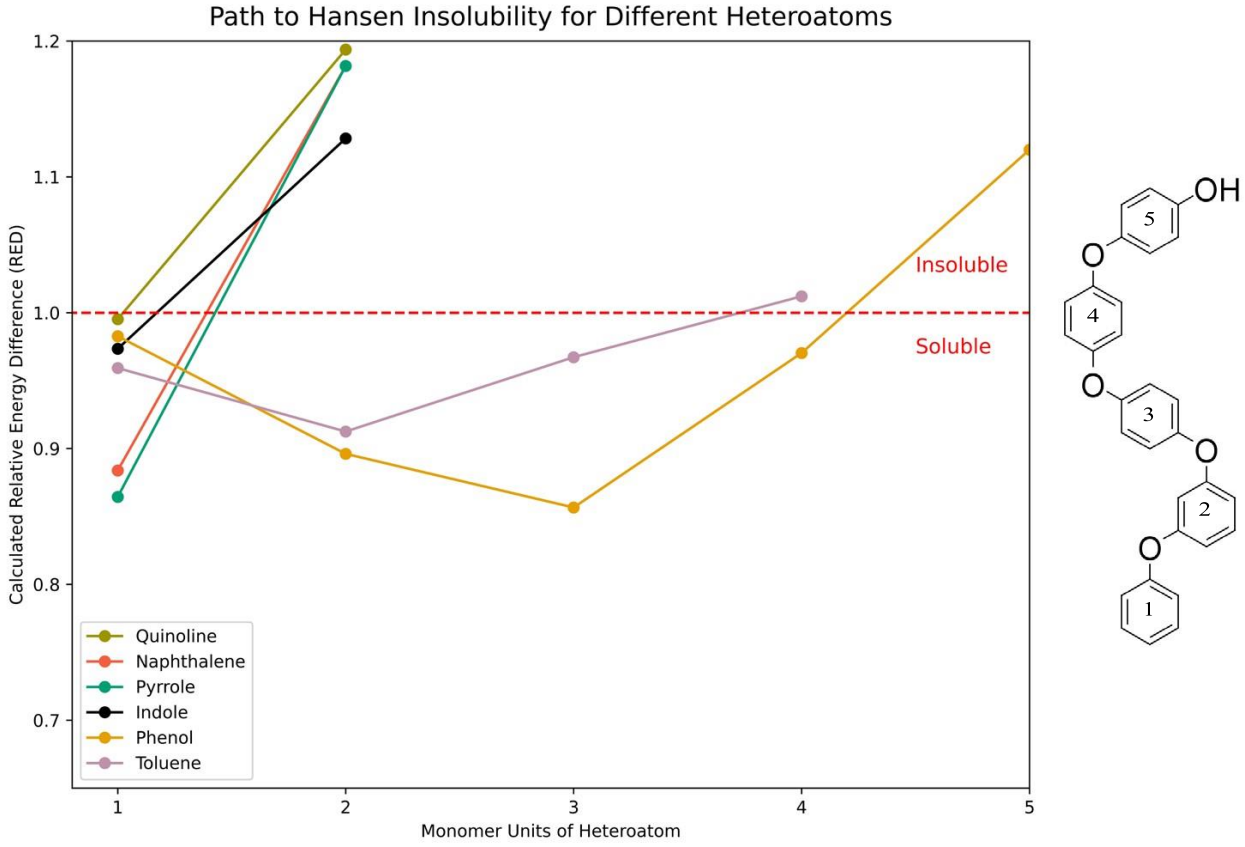

Figure 3.3: Effect of oligomer unit size on solubility calculated using the HSPiP software. It is clear some heteroatoms reach insoluble threshold in fewer units than others. Phenol and toluene is particularly interesting, becoming initially more soluble in *n*-dodecane before reaching the threshold. For phenol this is due to the growth of oligomer leading to a lower proportion of the molecule containing the *H*-bonding –OH group, but as the molecule grows the Van Der Waals dD difference grows eventually leading to an insoluble.

3.3 Predicting Deposition formation using DFT

3.3.1 H-abstraction and Coupling Mechanisms for Each Heteratom

Based on the solubility modelling presented in Figure 3.3, it was clear that the coupling of fuel heteratoms would lead to insoluble formation in our *n*-dodecane surrogate. Following the proposed HAS pathway, we calculated the H-abstraction and subsequent barriers to form dimers via the HAS pathway. The barriers for these reactions are presented in detail in Table S.1 of the appendix. The termination reaction was barrierless for all the species, and the pre-exponential factor was kept constant for each of the species at 3×10^9.[5]

The H-abstraction site and the coupling site for each species was selected based on literature and our own testing, and is summarized in Figure 3.4. For phenol, H-abstraction occurs at the O-site, with coupling between the subsequent phenoxy radical and the para-carbon site of a phenol.[38] For naphthalene, the C3 site was favored over the C2 position in terms of both abstraction and coupling barrier heights. For quinoline, the C2 site is the most favored site for coupling and H-abstraction, and the barriers for abstraction were lower at the C2 site compared to the C3 site.[44] For toluene, the para position was selected for coupling and H-abstraction based on our own testing and literature data.[45]

For indole and pyrrole, the favored coupling and H-abstraction site were found to be different. For indole, the N1 site was found to be the most favorable site for H-abstraction, but the C3 site is the most favored for coupling. Nevertheless, C–N linkages are detected very rarely and are found to be thermodynamically prohibited for indole oligomers.[46, 47] As a consequence, we compared the overall pathway to dimers at the C3 position via H-abstraction at the N1 and C3 positions. The results for the indole dimer formation calculations are found in Figure S.4 of the SI. Overall, the C3 H-abstraction pathway shows

the highest barriers. Therefore, the N1 H-abstraction pathway for indole was chosen. Similarly, for pyrrole, H-abstraction at the N1 position is favored, yet polypyrrole is formed of C2-C2 linkages.[40] Comparing both pyrrole coupling C2 coupling pathways with H-abstraction at the N1 or C2 position, presented in Figure S.3, both pathways have similar barrier heights. Nevertheless, the initial H-abstraction reaction at the N1 position is more favorable and leads to an intermediate I1b *G* 24.49 kcal mol^{-1} lower in energy that the C2 pathway. As a consequence, following the N1 pathway, pyrrole would have antiox-

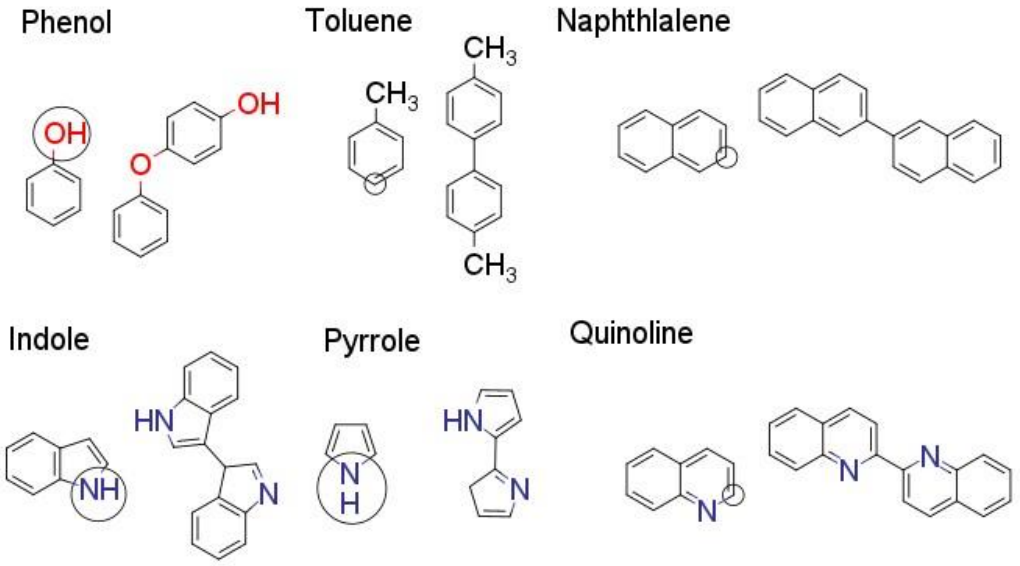

Figure 3.4: H-abstraction Sites and Dimers Selected for the Pseudo-Detailed Mechanisms. The selected H-abstraction site is circled, and resultant dimer is shown for each species.

idant properties, which is reflected in the petroOxy measurements (Figure 3.6b). Therefore the N1 abstraction pathway for pyrrole was chosen.

Regarding the different coupling and H-abstraction sites for indoles and pyrroles, it should be underlined that this difference may only be relevant to self-reactions. Indeed, for indole

and pyrrole functionalization reactions under oxidative conditions, the N- group is pre-protected prior to arylation and alkylation reactions. [52,40]

Based on the above proposed coupling and H-abstraction sites, we computed the barriers for ArH species reacting with *n*-dodecane R·,RO·, and ROO· radicals and subsequently forming dimers via a HAS process. The Gibbs potential energy surfaces for our chosen heteroatoms undergoing H-abstraction to the formation of dimers are presented in Figure 3.3 for RO·. The values for the reactions with the other radicals are presented in Table S.1 of the SI.

The first section (reaction A) of Figure 3.5, showing the abstraction of hydrogen from our selected ArH species. Here, we can see there is a clear difference in the reactivity and thermochemistry. To begin with, phenol shows the lowest barriers for hydrogen abstraction out of all the species tested. Phenol has long been known as a powerful antioxidant in fuels.[5] By contrast, toluene exhibits the highest barrier and the overall Gibbs energy abstraction reaction is endergonic at +28.32kcalmol ^{1}. The overall order of the Gibbs energy barrier to hydrogen abstraction (section A) is, in descending order: toluene > naphthalene > quinoline > pyrrole > indole > phenol.

The resultant radicals formed indicate that phenol, pyrrole, and indole all exhibit antioxidant properties, by undergoing an exergonic H-abstraction reactions. By contrast, naphthalene, toluene, and quinoline undergo endergonic H-abstraction reactions showing no antioxidant qualities. At this point in the reaction process, two Ar· radicals can terminate to form a dimer. Nevertheless, this termination process is a rare occurrence due to the low-concentration of Ar· species in fuel (for example, for pyrrole the peak concentration in our mechanism was 5.17E-13 mol l^{-1}).

The HAS reaction between an Ar· and ArH first proceeds with an attack of the radical. The radical attack is shown as pathway B) in Figure 3.5. For this step, the antioxidant species formation is endergonic and proceeds with high Gibbs energy barriers for phenol and indole of $‡G$ 25.63 kcal mol^{-1} and $‡G$=24.36 kcal mol^{-1} respectively. By contrast, pyrrole proceeds with a lower barrier of $‡G$=19.20 kcal mol^{-1}. On the other hand, the non-antioxidant species show lower barriers for pathway B). In fact, naphthalene and toluene show the highest barriers for the H-abstraction step, but lowest barriers out of all the species for step B) at $‡G$=12.87 kcal mol^{-1} and $‡G$=13.50 kcal mol^{-1} respectively. Additionally, the formation of the intermediate is the most exergonic for naphthalene and toluene. The relationship between the antioxidant tendency and the ease of coupling is likely related to the aromatic structure. Species with more antioxidant qualities will also have higher levels of aromaticity to stabilize radicals, but also will have higher barriers to aromaticity-breaking radical attack.

The final step in the dimer forming process is the re-aromatization step *via* loss of hydrogen from the intermediate. Interestingly, the barriers for this step are similar for our aromatics tested, in the range of 23.87-17.47 kcal mol^{-1}. This step is clearly less related to the structure of the ArH compound. Nevertheless, the concentration of ROOH available to complete this step, is related to the antioxidant qualities of the ArH species in fuels. For example, for phenols, due to their antioxidant properties, the concentration of ROOH is expected to be low.[24] As a consequence, termination reactions likely provide a higher source of C–C/C–O coupling. To explore how these interrelated pathways yield deposits for different fuel components, we created different pseudo-detailed mechanisms to compare each fuel.

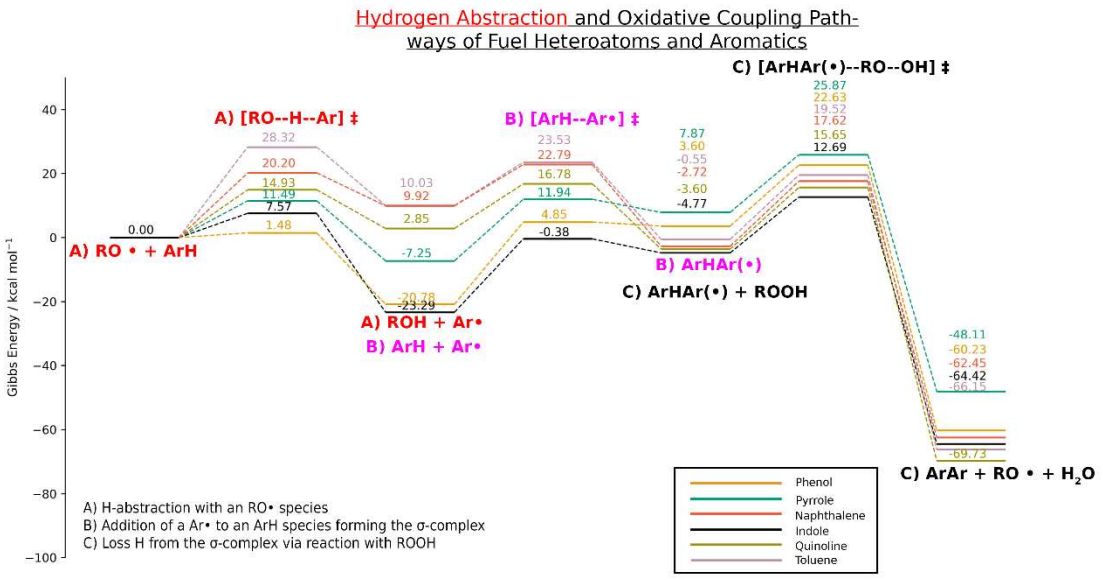

391

392 Figure 3.5: Growth to a deposit dimer for our chosen heteroatoms, calculated at the B3LYP-
393 D3/cc-pVTZ *n*-dodecane PCM level of theory. The barriers were calculated from stable pre-
394 reaction complexes. The R species was *n*-dodecane. The antioxidant species (phenol, indole
395 and pyrrole) show exergonic H-abstraction in step Ar.

396

397

398

399 3.3.2 Comparison of Experimental Results and Psuedo-Detailed Models

400 **Antioxidant Behavior**

401 First, the antioxidant behavior of our surrogate fuels was explored in relation to our models.
402 The O_2 depletion predicted by our model alongside the petroOxy depletion curves are
403 presented in Figure 3.6. Although the petroOxy device cannot measure the O_2 depletion in
404 the bulk, the device can be used to assess the antioxidant behavior of different fuels.[76] Our

model successfully predicts that pyrrole, indole, and phenol are all antioxidant species, as shown by the increased induction period in thepetroOxy curves. In addition, the petroOxy device indicates that indole and phenols are stronger antioxidants than pyrrole, which is also reflected in the O_2 depletion curves in our mechanism. However, the difference between indole and phenol in the petroOxy curves is not reflected in the mechanism. ~~Nevertheless, this difference between the surrogates is better reflected in the ArH + RO· abstraction barrier in Figure 3.5. Exploring the GCMS results for indole in our previous study, in Figure 10.22, no *n*-dodecane autoxidation products are observed after 8h. By contrast, pyrrole and quinoline both show lesser antioxidant qualities and lead to *n*-dodecane autoxidation products in Figure 5.7. Similarly, for our model, no oxygen is consumed leading to no autoxidation products.~~

Deposition Behavior

The amount of insoluble dimers predicted by our model compared with the total insolubles measured is presented in Figure 3.7. It should be noted that the comparison here is focused on the *correlation* between amount of dimers predicted and total deposit produced by experiment. As a consequence, the correlation produced will reflect how well the model predicts deposition behavior. Indeed, the difference between correlated and measured deposits by a factor of ~300. This is due to the fact our mechanism only focuses on the formation of dimers. Dimers are likely only to form a small proportion of the total deposit structure, hence the large different in mass. Instead, the results here intend to explore how well the model predicts couple propensity between different species which we hypothesize is related to the ease of forming dimers. The model predicts the insoluble formation behavior between our different surrogates well, with pyrrole producing the largest amounts of insolubles. Interestingly, phenol and indole are shown to produce the lowest amount of

deposit in both our experiments and model. By contrast, in real fuels, indoles, and particularly phenol concentration are shown to correlate well with final insoluble mass.[8] A key difference between our simplified surrogates and real fuels are the synergistic effects between fuel classes, which are not captured in our two-component surrogates. In particular, sulfur is shown to interact strongly with 5-membered nitrogen heterocycles, and phenols with other nitrogen compounds.[7, 48] For example, in a simplified surrogate, previous work has shown trends between deposition propensity of 5- and 6-membered heterocycles break down, where quinoline-like compounds have shown to produce more deposit than indole compounds.[7] Nevertheless, the use of surrogates is still important to understand the chemical interactions within species classes.

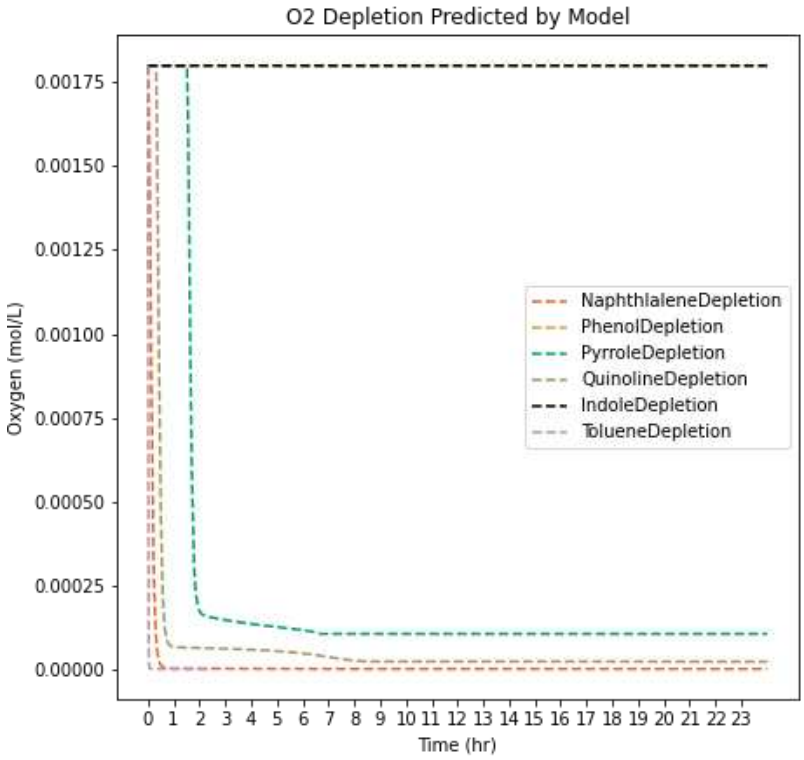

(a) O_2 Depletion Predicted by our model

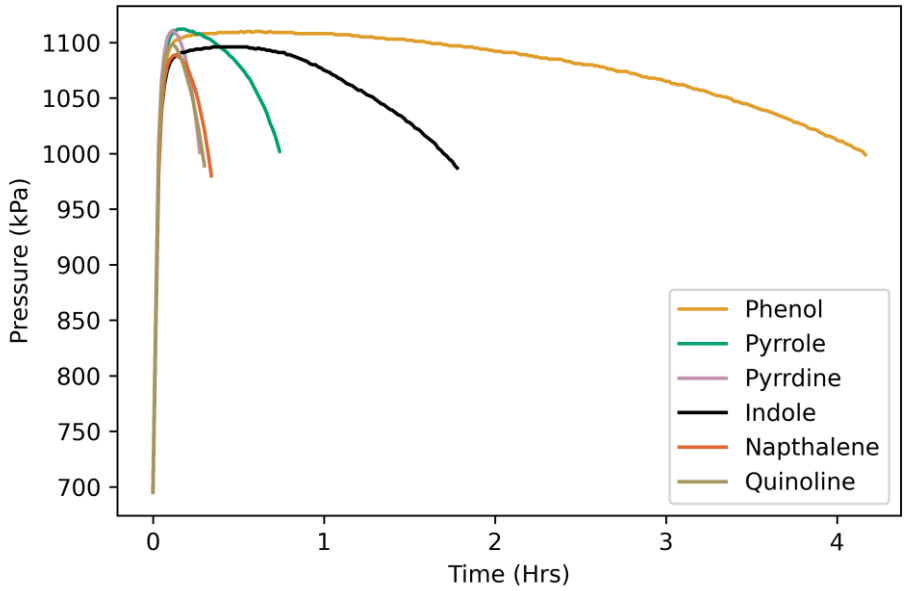

(b) Petroxy depletion behavior

Figure 3.6: O_2 depletion behavior of our surrogate- comparison between model and experiment. The model shows the change in O_2 concentration over time. The petroOxy depletion curves show the change in headspace pressure, and although they are not a direct measure of O_2 depletion, they can differentiate between antioxidant qualities of different species.

Interestingly, in our experiment and models, toluene and naphthalene produced more insolubles than phenol and indole. This is interesting as fuel thermal degradation is often viewed as solely driven by heteroatoms.[25] Exploring the barriers for toluene and naphthalene in detail in Table S.1, we see that lower barriers to the ArH + Ar·→ ArHAr· reaction are found with the aromatic species. Sensitivity analysis (Figure 3.9) of our models suggests this coupling step is strongly related to the final insoluble mass. However, in a 2-component fuel, combining an antioxidant heteroatom and aromatic, the formation of aromatic insolubles will be significantly reduced due to the size of the H-abstraction barrier in comparison to the other heteroatoms used in this study (Figure 3.5). Instead, the

457 heteroatom antioxidant class will form the majority of the Ar· radicals going on to form
458 deposit. To strengthen this hypothesis, using our calculated values, a fuel model was built
459 containing both phenol and toluene.

460 The effect of heteroatoms suppressing deposition from non-antioxidant species is
461 demonstrated in Figure 3.8, where insolubles are generated from pseudo-detail model fuels
462 containing different ratios of toluene and phenol is tested. The model was built using the
463 same BAS scheme base described in the section 2.4, with the addition of both toluene and
464 phenol pathways. In this simplified model, toluene-derived insolubles are suppressed upon
465 introduction of phenol. This effect can help explain why fuel deposits/insolubles often have
466 an elemental composition of heteroatoms higher than conventional fuels also containing
467 aromatic hydrocarbons.[49] Another interesting effect of blending is the peak in phenol
468 insolubles at 25:75 phenol:toluene ratios above a 100% phenol mix, which implies that above
469 a certain concentration, phenols will prevent the formation of insolubles. The peak
470 concentration of hydroperoxide steadily drops at different % phenol concentrations, which
471 is related to the extent the autoxidation chain is suppressed. The peak of phenol deposition
472 could be related to the ROOH concentration, allowing more σ-intermediates to be re-
473 aromatized. This shows our model can replicate the effect of changing concentrations of
474 antioxidant on total insolubles.

475 For some of the fuels the pseudo-detailed mechanisms reflect the behavior of 'peak'
476 deposition temperature. The effect of temperature on the concentration of deposits for each
477 mechanism is shown in Figures S.6-10 of the SI. For quinoline, a peak deposition level is
478 reached at 460K. Whereas for toluene, as the temperature increases the level of deposit
479 decreases. All the other fuel models show an increase in concentration of deposit as the
480 temperature rises. This demonstrates these deposit mechanisms can reflect the complex

behavior of observed in real fuels of increasing and decreasing levels of deposit depending on fuel temperature.[50]

Finally, our results here lend credence to a HAS pathway leading to deposit. When the HAS pathway is removed from the mechanism in Figure 3.7b, no discernable trend is found between the formation of dimers and insolubles measured. In fact, the HAS pathway appears particularly important for species with low/no antioxidant tendency, but with a tendency to still form insolubles.

Sensitivity analysis of our bespoke mechanisms in presented in Figure 3.9. The reaction numbers cited here correspond to those given in Table S.1. For our mechanisms, the reaction 29, Ar· + ArH → ArHAr·, has the largest influence on the level of deposit with the exception of phenol. Increasing the rate of reaction 29 leads to more ArHAr· species which can readily form deposit. Reaction 32, Ar· + ROOH → ArH + ROO·, removing hydroperoxides from the system also has an influence on the level of deposit. As the rate of reaction 32 increases, hydroperoxides are removed from the system leading to fewer ArHAr· + ROOH re-aromatization reactions leading to deposit dimers. The change of ROOH and insoluble concentration presented in Figure 3.10 demonstrates that as insolubles are produced ROOH is depleted. For all the species tested, the RO· (reaction 26) and R· (reaction 27) hydrogen abstraction steps have a large influence on the level of deposit, with faster rates leading to more Ar· species able to undergo coupling reactions. By contrast, the rate of the ROO· abstraction barrier (reaction 16) has a negligible influence on deposition for most species because this reaction in general has high barriers already. Finally, for phenol, reaction 26, ArH + R→ Ar· + RH also influences the formation of deposit more than the other species, and is more important than the coupling step (reaction 29). This is likely because the

termination pathway dominates the formation of deposits here, thus leading to a direct correlation between the concentration of Ar· and the amount of deposit dimer.

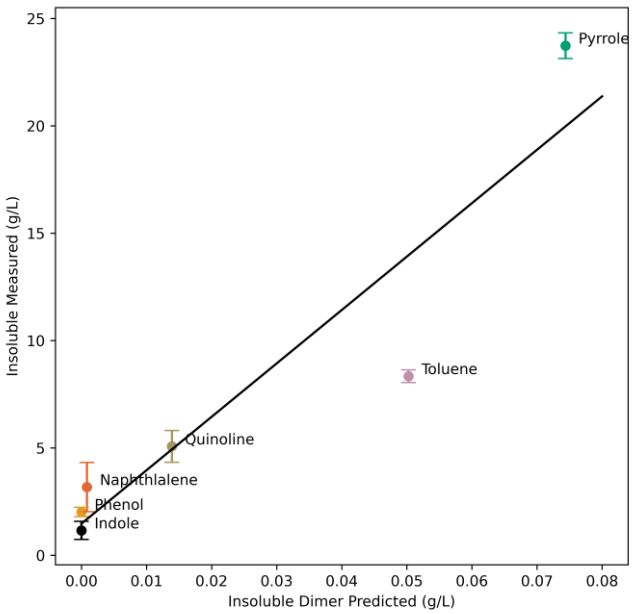

(a) Correlation between mass of dimer predicted by our model and insolubles measured.

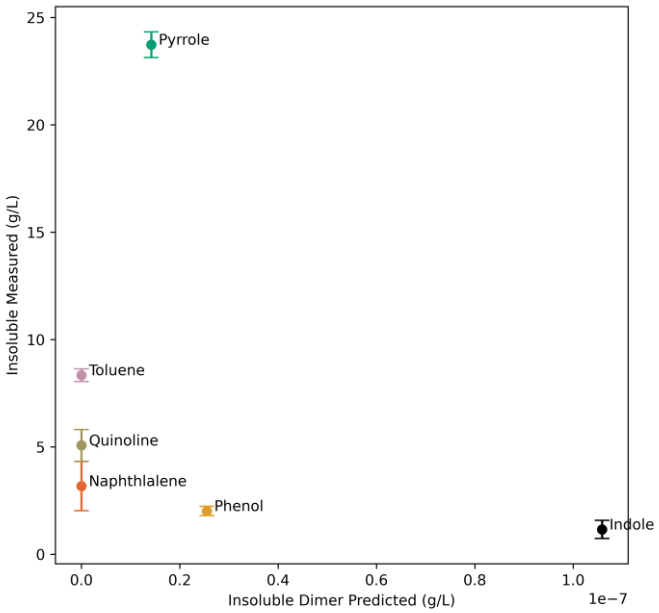

(b) Correlation between mass of dimer predicted by our model and insolubles measuredwhen the HAS pathway is excluded.

Figure 3.7: Insoluble formation behavior- comparisons between model and experiment. Temperature of the experiment and psuedo-detailed *n*-dodecane chemical mechanism containing the A and E_a values shown in Table S.1. The temperature was set at 431 K both the model and the experiment.

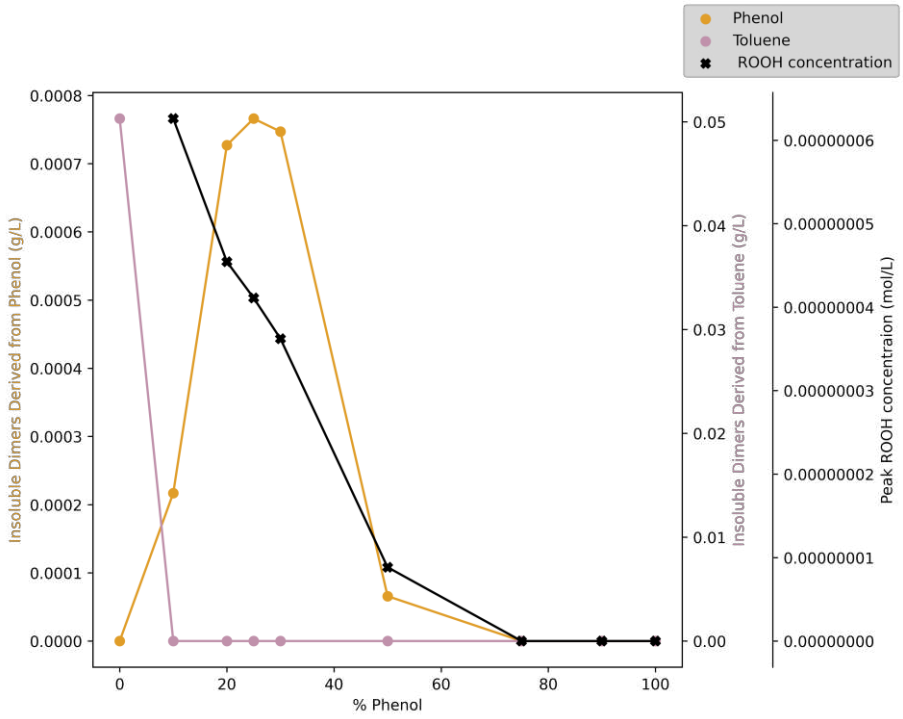

Figure 3.8: Effect of phenol % in a phenol toluene aromatic total of 0.1 mol L^{-1} on the insolubles derived from phenol and toluene.

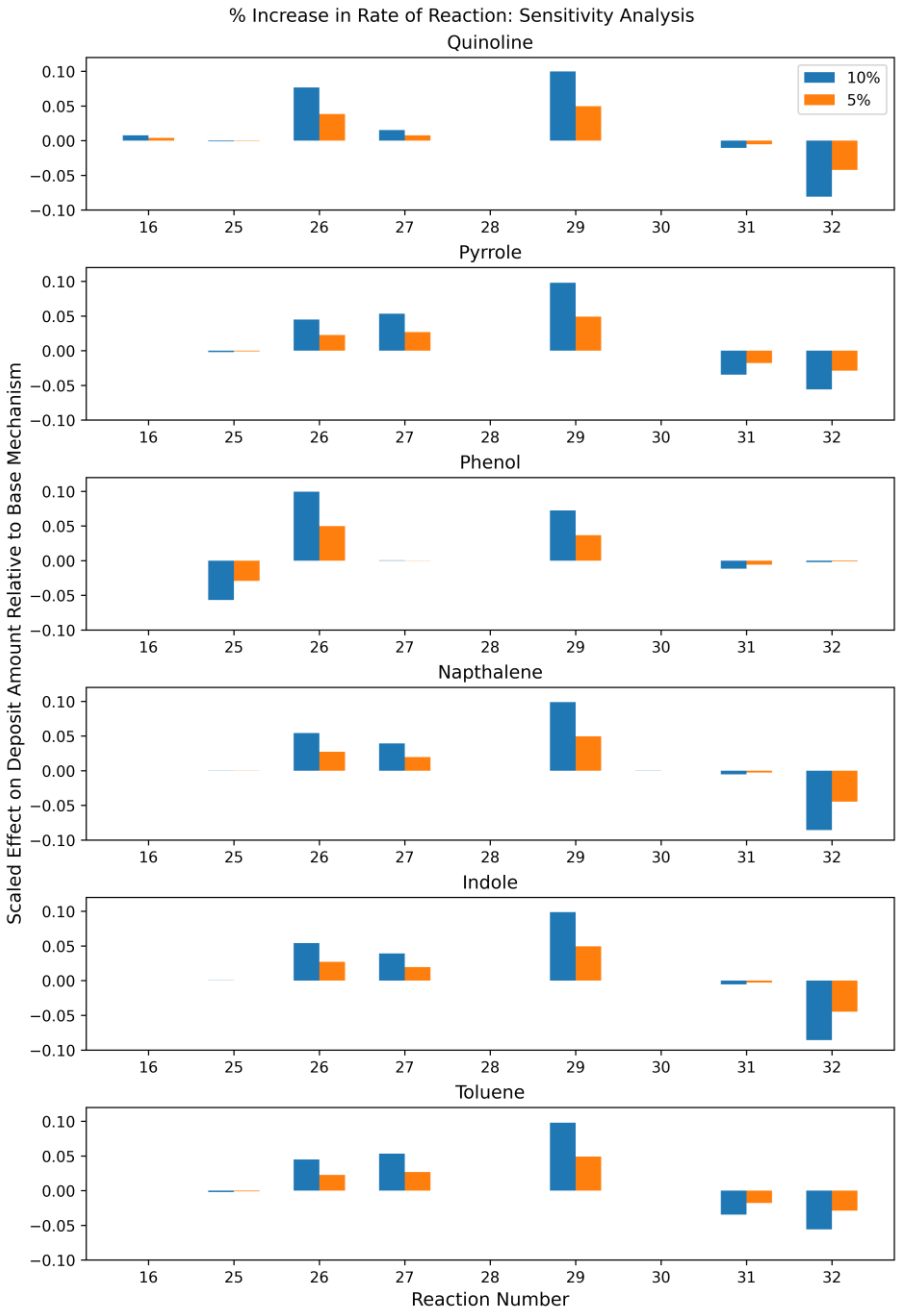

Figure 3.9: Sensitivity analysis of the bespoke insoluble pseudo-detailed mechanisms. For the sensitivity analysis, the rate of reaction is increased by a factor of 10% (blue) and 5% (orange) and the resultant increase in insolubles is shown relative to the base pseudo-detailed mechanism. The reaction number corresponds to Table S.1 in the SI

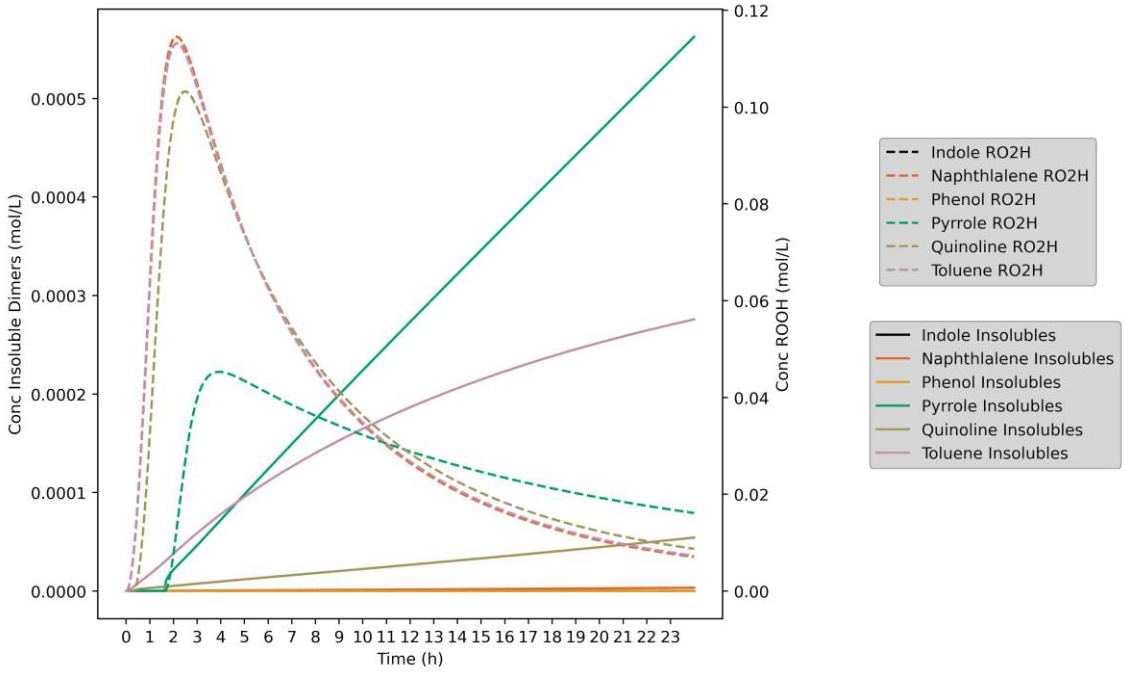

Figure 3.10: Change in the concentration of insolubles and ROOH over the course of the 24h pseudo-detailed models. The thick lines show the change in insoluble dimer concentration, whereas the dotted lines show the change in ROOH concentration. The results clearly show that for each species, as ROOH is depleted, the level insolubles begin to increase.

3.4 Implication for Fuels

A key novel finding of this study is the role that HAS reactions can play in deposit formation. Additionally, the work here represents the first study to apply DFT calculations to deposition reactions to attempt to predict deposition tendency from first principles.

One weakness of this study is that it looked solely into aromatic self-reactions via the HAS process, whereas side reactions between ArH and RH species will be dominant in a

real fuel scenario due to the low concentration of ArH in real-fuels. To briefly explore side reactions, we calculated the initial step of a HAS pathway between propanal, and various nitrogen compounds which is presented in Figure S.5 of the SI. In this pathway, propanal readily forms a σ-intermediate with the nitrogen heteroatoms. Future studies should explore the HAS pathway for fuel-aromatic side reactions, particularly as no mechanism is currently proposed in the fuel literature which does not rely on a termination step to form the C-C bond or without unrealistic EAS steps forming charged intermediates.[52]

The formation of fuel insolubles is influenced by both the H-abstraction and coupling propensity of the heteroatoms/aromatics present in fuel. By simplifying the insoluble formation process into the formation of dimers, we were able to show clear differences between the insoluble formation and antioxidant tendency between surrogate fuels. Nevertheless, the formation of dimers represents a small subsection of the insoluble/deposit structure. To expand the mechanism to reach an insolubles formation model which can provide a quantitatively accurate description, additional pathways need to be considered. This is a challenge, particularly as there are likely thousands of possible side reactions between and within species classes.[2] Even in our surrogate fuels the oxidation of *n*-dodecane is not significantly repressed.

To address the challenge of building a branching deposition mechanism with thousands of reactions, several approaches using techniques benchmarked in this study can be used. The first approach involves scaling the deposit forming dimer steps to experimental deposit measurements. This would lead to a semi-empirical mechanism, which moves

away from the first-principles approach using DFT. Nevertheless, the DFT thermochemical and kinetic parameters will allow the gross differences between species class and structure to be explored. This approach relies on the assumption that the formation of deposit dimers relates to a general property of 'coupling propensity'. Some preliminary calculations imply this assumption is generally correct, where a propanal doublet attacking various nitrogen compounds give barrier sizes (presented in Figure S.5 in the SI) in the same order of magnitude as the dimerization barriers for step B) in Figure 3.5.

A second, more computationally intensive approach, would be a set of high throughput calculations on additional deposit forming pathways. This approach would use HAS and termination reactions to calculate the pathways to various oligomers. These reactions could be constructed following chemical graph theory, as employed in recent work with phenols.[53] Hansen solubility parameters will guide a 'cut-off' point for energetic pathways to oligomers to form insolubles. Nevertheless, insoluble species are still likely to react to form larger molecular weight species, which adds an additional challenge to this approach.

Declaration of Interest

This research was partly funded by the University of Sheffield Department of Mechanical Engineering, PhD Scholarship Scheme, and the Powerplant Integration of Novel Engine Systems (PINES) grant number 113263.

4.5 Conclusions

The formation of insolubles in fuel is driven by coupling reactions between aromatics. In this work we have shown the importance of HAS in explaining the formation of these insolubles. DFT calculations revealed that the hydroperoxides play a key role in facilitating the HAS pathway. As a result of these findings, we showed that kinetic values calculated for a simplified two-component (dodecane and aromatic) surrogate can reveal differences in antioxidant and deposition tendency of different aromatics compared to the experiment. In addition, when the HAS pathway is excluded, the predicted deposition trends break down. Exploring the behavior of the mechanism further, we show that the addition of antioxidant to an antioxidant+aromatic model leads the suppression of insolubles composed of the aromatic. Instead, the antioxidant+aromatic model leads to insolubles only composed of the antioxidant. Finally, sensitivity analysis reveals that the formation of hydroperoxides ($ArH + ROO \rightarrow Ar\cdot + ROOH$) and the homolytic coupling ($ArH + Ar\cdot \rightarrow ArHAr\cdot$) have a strong influence on the final deposit mass.

BIBLIOGRAPHY

1- T. Jia, L. Pan, S. Gong, J. Xie, X. Wang, Y. Fang, J. J. Zou, and X. Zhang, "Mechanistic insights into the thermal deposition of highly thermal-stable jet fuel," *Fuel*, vol. 276, no. May, p. 118100, 2020.

2- M. Commodo, I. Fabris, C. P. T. Groth, and Ö. L. Gülder, "Analysis of aviation fuel thermal oxidative stability by electrospray ionization mass spectrometry (ESI-MS)," *Energy and Fuels*, vol. 25, no. 5, pp. 2142–2150, 2011.

3- S. P. Heneghan and S. Zabarnick, "Oxidation of jet fuels and the formation of deposit," *Fuel*, vol. 73, pp. 35–43, jan 1994.

4- F. R. Mayo and B. Y. Lan, "Gum and deposit formation from jet turbine and diesel fuels at 130.degree.C," *Industrial Engineering Chemistry Product Research and Development*, vol. 25, pp. 333–348, jun 1986.

5- N. J. Kuprowicz, S. Zabarnick, Z. J. West, and J. S. Ervin, “Use of measured species class concentrations with chemical kinetic modeling for the prediction of autoxidation and deposition of jet fuels,” *Energy and Fuels*, vol. 21, no. 2, pp. 530–544, 2007.

6- R. H. Clark and L. Smith, “Further studies of the effects of polar compounds on the thermal stability of jet fuel,” in *3rd International Conference on Stability And Handling of Liquid Fuels*, no. 2, 1988.

7- S. Zabarnick, Z. J. West, L. M. Shafer, S. S. Mueller, R. C. Striebich, and P. J. Wrzesinski, “Studies of the role of heteroatomic species in jet fuel thermal stability: model fuel mixtures and real fuels,” *Energy and Fuels*, vol. 33, no. 9, pp. 8557–8565, 2019.

8- L. M. Balster, S. Zabarnick, R. C. Striebich, L. M. Shafer, and Z. J. West, “Analysis of polar species in jet fuel and determination of their role in autoxidative deposit formation,” *Energy and Fuels*, vol. 20, no. 6, pp. 2564–2571, 2006.

9- M. Grzybowski, K. Skonieczny, H. Butenschön, and D. T. Gryko, “Comparison of oxidative aromatic coupling and the scholl reaction,” *Angewandte Chemie - International Edition*, vol. 52, no. 38, pp. 9900–9930, 2013.

10- P. D. McDonald and G. A. Hamilton, *Mechanisms of Phenolic Oxidative Coupling Reactions*, vol. 5. Academic Press, INC., 1973.

11- W. R. Bowman and J. M. Storey, “Synthesis using aromatic homolytic substitution—recent advances,” *Chemical Society Reviews*, vol. 36, no. 11, pp. 1803–1822, 2007.

12- C.-L. Sun and Z.-J. Shi, “Transition-metal-free coupling reactions,” *Chemical Reviews*, vol. 114, no. 18, pp. 9219–9280, 2014. PMID: 25184859.

13- M. Monge-Palacios, E. Grajales-González, G. Kukkadapu, and S. M. Sarathy, “Kinetics of the benzyl + HO2and benzoxyl + OH barrierless association reactions: fate of the benzyl hydroperoxide adduct under combustion and atmospheric conditions,” *Physical Chemistry Chemical Physics*, vol. 22, no. 16, pp. 9029–9039, 2020.

14- F. Minisci, “Recent aspects of homolytic aromatic substitutions.,” *Topics in current chemistry*, vol. 62, pp. 1–48, 1976.

15- B. Beaver, L. Gao, C. Burgess-Clifford, and M. Sobkowiak, “On the mechanisms of formation of thermal oxidative deposits in jet fuels. Are unified mechanisms possible for both storage and thermal oxidative deposit formation for middle distillate fuels?,” *Energy and Fuels*, vol. 19, no. 4, pp. 1574–1579, 2005.

16- T. Stuyver, D. Danovich, F. De Proft, and S. Shaik, “Electrophilic Aromatic Substitution Reactions: Mechanistic Landscape, Electrostatic and ElectricField

650 Control of Reaction Rates, and Mechanistic Crossovers," *Journal of the*
651 *American Chemical Society*, vol. 141, no. 24, pp. 9719–9730, 2019.

652 17- D. P. Curran and A. I. Keller, "Radical additions of aryl iodides to arenes are
653 facilitated by oxidative rearomatization with dioxygen," *Journal of the*
654 *American Chemical Society*, vol. 128, no. 42, pp. 13706–13707, 2006.

655 18- R. Venkataraman and S. Eser, "Characterisation of solid deposits from the
656 thermal-oxidative degradation of jet fuel," *International Journal of Oil, Gas*
657 *and Coal Technology*, vol. 1, no. 1-2, pp. 126–137, 2008.

658 19- O. Altin and S. Eser, "Carbon deposition from thermal stressing of petroleum
659 fuels," *ACS National Meeting Book of Abstracts*, vol. 228, no. 1, 2004.

660 20- Z. Liu, S. Tang, Z. Li, Z. Qin, S. Yuan, L. Wang, L. Wang, X. Zhang, and G.
661 Liu, "An improved kinetic model for deposition by thermal oxidation of
662 aviation hydrocarbon fuels," *Fuel*, vol. 258, no. June, p. 116139, 2019.

663 21- C. M. Parks, A. J. Meijer, S. G. Blakey, E. Alborzi, and M. Pourkashanian,
664 "Computational studies on the reactions of thiols, sulfides and disulfides with
665 hydroperoxides. Relevance for jet fuel autoxidation," *Fuel*, vol. 316, no.
666 January, p. 123326, 2022.

667 22- E. Alborzi, M. R. Dwyer, C. M. , A. Sheikhansari, D. C. Mielczarek, M.
668 Zanganeh, A. J. Meijer, S. G. Blakey, and M. Pourkashanian, "Construction of

669 a reduced chemical kinetic mechanism for autoxidation of n-paraffinic solvent
670 – A model for aviation fuel," *Fuel*, vol. 294, no. January, p. 120170, 2021.

671 23- A. C. Antoine, "EFFECT OF SOME NITROGEN COMPOUNDS ON
672 THERMAL STABILITY OF JET A.," *NASA Technical Memorandum*, jun
673 1982.

674 24- L. Jones and N. C. Li, "Ageing of SRC II middle distillate from Illinois No. 6
675 coal," *Fuel*, vol. 62, no. 10, pp. 1156–1160, 1983.

676 25- R. N. Hazlett and A. J. Power, "Phenolic compounds in Bass Strait distillate
677 fuels: their effect on deposit formation," *Fuel*, vol. 68, no. 9, pp. 1112–1117,
678 1989.

679 26- T. Jia, M. Zhao, L. Pan, C. Deng, J.-j. Zou, and X. Zhang, "Effect of phenolic
680 antioxidants on the thermal oxidation stability of high-energy-density fuel,"
681 *Chemical Engineering Science*, p. 117056, 2021.

682 27- John M. Andrésen, James J. Strohm, , Lu Sun, and C. Song*, "Relationship
683 between the Formation of Aromatic Compounds and Solid Deposition during
684 Thermal Degradation of Jet Fuels in the Pyrolytic Regime," 2001.

685 28- S. Jain and M. P. Sharma, "Review of different test methods for the evaluation
686 of stability of biodiesel," *Renewable and Sustainable Energy Reviews*, vol. 14,
687 no. 7, pp. 1937–1947, 2010.

29- M. J. Frisch, G. W. Trucks, H. B. Schlegel, G. E. Scuseria, M. A. Robb, J. R. Cheeseman, G. Scalmani, V. Barone, B. Mennucci, G. A. Petersson, H. Nakatsuji, M. Caricato, X. Li, H. P. Hratchian, A. F. Izmaylov, J. Bloino, G. Zheng, J. L. Sonnenberg, M. Hada, M. Ehara, K. Toyota, R. Fukuda, J. Hasegawa, M. Ishida, T. Nakajima, Y. Honda, O. Kitao, H. Nakai, T. Vreven, J. A. Montgomery, Jr., J. E. Peralta, F. Ogliaro, M. Bearpark, J. J. Heyd, E. Brothers, K. N. Kudin, V. N. Staroverov, R. Kobayashi, J. Normand, K. Raghavachari, A. Rendell, J. C. Burant, S. S. Iyengar, J. Tomasi, M. Cossi, N. Rega, J. M. Millam, M. Klene, J. E. Knox, J. B. Cross, V. Bakken, C. Adamo, J. Jaramillo, R. Gomperts, R. E. Stratmann, O. Yazyev, A. J. Austin, R. Cammi, C. Pomelli, J. W. Ochterski, R. L. Martin, K. Morokuma, V. G. Zakrzewski, G. A. Voth, P. Salvador, J. J. Dannenberg, S. Dapprich, A. D. Daniels, Ö. Farkas, J. B. Foresman, J. V. Ortiz, J. Cioslowski, and D. J. Fox, "Gaussian 09 Revision E.01," 2009. Gaussian Inc. Wallingford CT 2009.

30- A. D. Becke, "Density-functional thermochemistry. III. The role of exact exchange," *The Journal of Chemical Physics*, vol. 98, no. 7, pp. 5648–5652, 1993.

31- S. Grimme, S. Ehrlich, and L. Goerigk, "Effect of the damping function in dispersion corrected density functional theory," *Journal of computational chemistry*, vol. 32, no. 7, pp. 1456–1465, 2011.

32- S. Miertuš, E. Scrocco, and J. Tomasi, “Electrostatic interaction of a solute with a continuum. a direct utilizaion of ab initio molecular potentials for the prevision of solvent effects,” *Chemical Physics*, vol. 55, no. 1, pp. 117–129, 1981.

33- T. H. Dunning Jr, “Gaussian basis sets for use in correlated molecular calculations. i. the atoms boron through neon and hydrogen,” *The Journal of chemical physics*, vol. 90, no. 2, pp. 1007–1023, 1989.

34- S. Grimme, “Supramolecular binding thermodynamics by dispersion-corrected density functional theory,” *Chemistry–A European Journal*, vol. 18, no. 32, pp. 9955–9964, 2012.

35- R. F. Ribeiro, A. V. Marenich, C. J. Cramer, and D. G. Truhlar, “Use of solution-phase vibrational frequencies in continuum models for the free energy of solvation,” *The Journal of Physical Chemistry B*, vol. 115, no. 49, pp. 14556–14562, 2011.

36- R. Paton, “Goodvibes,” 2016.

37- S. Zabarnick, “Chemical kinetic modeling of jet fuel autoxidation and antioxidant chemistry,” *Industrial Engineering Chemistry Research*, vol. 32, pp. 1012–1017, jun 1993.

38- S. Kobayashi and H. Higashimura, “Oxidative polymerization of phenols revisited,” *Progress in Polymer Science (Oxford)*, vol. 28, no. 6, pp. 1015–1048, 2003.

39- S. Baena-Zambrana, S. L. Repetto, C. P. Lawson, and J. K. Lam, “Behaviour of water in jet fuel - A literature review,” *Progress in Aerospace Sciences*, vol. 60, pp. 35–44, 2013.

40- J. K. Howard, K. J. Rihak, A. C. Bissember, and J. A. Smith, “The Oxidation of Pyrrole,” *Chemistry - An Asian Journal*, vol. 11, no. 2, pp. 155–167, 2016.

41- Z. Zhang, X. Yue, Y. Duan, and Z. Rao, “A study on the mechanism of oxidized quinoline removal from acid solutions based on persulfate-iron systems,” *RSC Advances*, vol. 10, no. 21, pp. 12504–12510, 2020.

42- J. D. Mosley, A. M. Ricks, P. V. Schleyer, J. I. Wu, and M. A. Duncan, “IR spectroscopy of ↵ And -protonated pyrrole via argon complex photodissociation,” *Journal of Physical Chemistry A*, vol. 116, no. 39, pp. 9689–9695, 2012.

43- M. J. DeWitt, Z. West, S. Zabarnick, L. Shafer, R. Striebich, A. Higgins, and T. Edwards, “Effect of Aromatics on the Thermal-Oxidative Stability of Synthetic Paraffinic Kerosene,” *Energy & Fuels*, vol. 28, pp. 3696–3703, jun 2014.

44- S. Zabarnick, “Chemical kinetic modeling of jet fuel autoxidation and antioxidant chemistry,” *Industrial Engineering Chemistry Research*, vol. 32, pp. 1012–1017, jun 1993.

45- . Wang, A. Violi, D. H. Kim, and J. A. Mullholland, “Formation of naphthalene, indene, and benzene from cyclopentadiene pyrolysis: A DFT study,” *Journal of Physical Chemistry A*, vol. 110, no. 14, pp. 4719–4725, 2006.

46- Zotti, G., Zecchin, S., Schiavon, G., Seraglia, R., Berlin, A., & Canavesi, A. (1994). Structure of Polyindoles from Anodic Coupling of Indoles: An Electrochemical Approach. Chemistry of Materials, 6(10), 1742–1748. https://doi.org/10.1021/cm00046a029 P. J. Steel, “Aromatic biheterocycles: Syntheses, structures, and properties,” *Advances in heterocyclic chemistry*, vol. 67, pp. 2–118, 1997.

47- Talbi, H., Monard, G., Loos, M., & Billaud, D. (1998). Theoretical study of indole polymerization. Journal of Molecular Structure: THEOCHEM, 434(1–3), 129–134. https://doi.org/10.1016/S0166-1280(98)00092-X

48- R. N. Hazlett, J. A. Schreifels, W. M. Stalick, R. E. Morris, and G. W. Mushrush, “Distillate fuel insolubles: formation conditions and characterization,” *Energy and Fuels*, vol. 5, no. 2, pp. 269–273, 1991.

49- Z., Steven, P. Zelesnik, and P. R. Grinstead. "Jet fuel deposition and oxidation: dilution, materials, oxygen, and temperature effects." *Turbo Expo: Power for*

765 *Land, Sea, and Air*. Vol. 78804. American Society of Mechanical Engineers,
766 1995.

767 50- Hazlett, R. N. (1991). Thermal Oxidation Stability of Aviation Turbine Fuels.
768 In Thermal Oxidation Stability of Aviation Turbine Fuels.
769 https://doi.org/10.1520/mono1-eb

770 51- Liu, S., Zhao, F., Chen, X., Deng, G. J., & Huang, H. (2020). Aerobic
771 Oxidative Functionalization of Indoles. Advanced Synthesis and Catalysis,
772 362(18), 3795–3823. https://doi.org/10.1002/adsc.202000285

773 52- Adams, C., Alborzi, E., Meijer, A. J. H. M., Hughes, K. J., & Pourkashanian,
774 M. (2023). Mechanistic investigation into the formation of insolubles in bulk
775 fuel jet fuel using quantum chemical and experimental techniques. Fuel,
776 334(P1), 126202. https://doi.org/10.1016/j.fuel.2022.126202

777 53- Raza, Z., Naz, K., & Ahmad, S. (2022). Expected Values of Molecular
778 Descriptors in Random Polyphenyl Chains. Emerging Science Journal, 6(1),
779 151–165. https://doi.org/10.28991/ESJ-2022-06-01-012

780

781

Declaration of interests

☐The authors declare that they have no known competing financial interests or personal relationships that could have appeared to influence the work reported in this paper.

☒The authors declare the following financial interests/personal relationships which may be considered as potential competing interests:

Charlie Adams reports financial support was provided by The University of Sheffield Department of Mechanical Engineering.